Constraining the vertical particle export during the last glacial cycle in Southern Indian Ocean sediment core

Master's Thesis

Faculty of Science

University of Bern

Presented by

Antoine Thévenaz

2019

Supervisor:

Prof. Samuel L. Jaccard

Institute of Geology, Oeschger Centre for Climate Change Research, University of Bern

Advisor:

Eri Amsler

Institute of Geology, Oeschger Centre for Climate Change Research, University of Bern

1. Abstract

The large, 80-100 ppm, glacial-interglacial variations in atmospheric CO_2 concentrations are today relatively well understood. However, low sediment accumulation in open ocean sediment cores generally prevents a fine, detailed comparison between marine and ice core records, in particular during ice ages. Core MD12-3394, retrieved from the Indian sector of the Southern Ocean, presents a very high sediment accumulation rate, which makes it possible to study in more details the climate-carbon cycle feedbacks during Marine Isotope Stage 3 (MIS 3) using a highly-resolved sedimentary archive. The thorium normalization method has been used to derive biogenic and lithogenic fluxes accounting for sediment focusing. Biogenic fluxes derived from XRF scanner measurements have been used as proxy for biological productivity. Temperature and atmospheric CO_2 concentration reconstructions from the Vostok and EPICA Dome C Antarctic ice cores have been compared with the proxies derived from the sediment core. The results show an overall low lithogenic flux in this core, which can be explained by its isolation. The lithogenic flux was particularly low during warm periods, and higher during cold periods. It peaked during the coldest periods of MIS 3. The biogenic fluxes are almost at zero during cold periods, and increase drastically when the climate became warmer. The opposite behavior of lithogenic flux and biogenic fluxes during warming phases, reducing lithogenic flux and increasing biogenic fluxes, point to an increasing upwelling enhancing the biological productivity. These results show that increased upwelling that contributed to the deglacial rise of atmospheric CO_2 was also active during the smaller-scale warming periods within the last ice age. This implies that the underlying mechanisms controlling the upwelling in the Southern Ocean, and by inference the transfer of previously sequestered CO_2 to the atmosphere, are reactive on a submillennial scale.

Table of Contents

2. Introduction

2.1. History of ice ages and their triggers

Ice ages are long periods during which Earth's average temperature was much lower than what we experience today, with a global average of around 4°C cooler during the coldest period of the last ice age (Annan & Hargreaves, 2013). Earth has had ice ages for the majority of the Quaternary, each lasting between 50,000 and 100,000 years, with short interglacials in between. The succession of longer, colder periods and shorter, warmer periods is due to variations in orbital parameters (Berger, 1992). The latitudinal, or seasonal, distribution of incoming solar radiation is directly influenced by the natural variations in Earth's orbit and rotation angle. A slight decrease in incoming solar radiations in the north hemisphere in summer, and snow can accumulate in greater areas. This leads to the growing of ice caps, and eventually an ice age as feedbacks enter into play. These feedbacks include, among others, the ice-albedo feedback. Ice and snow have a much higher albedo than soil or vegetation. As a result, a bigger fraction of the incoming solar radiation is directly reflected towards space. Thus, the temperature is lower where ice covers the ground, which contributes to the growing of ice caps. This is known as a positive feedback loop, as its effects increase the initial signal.

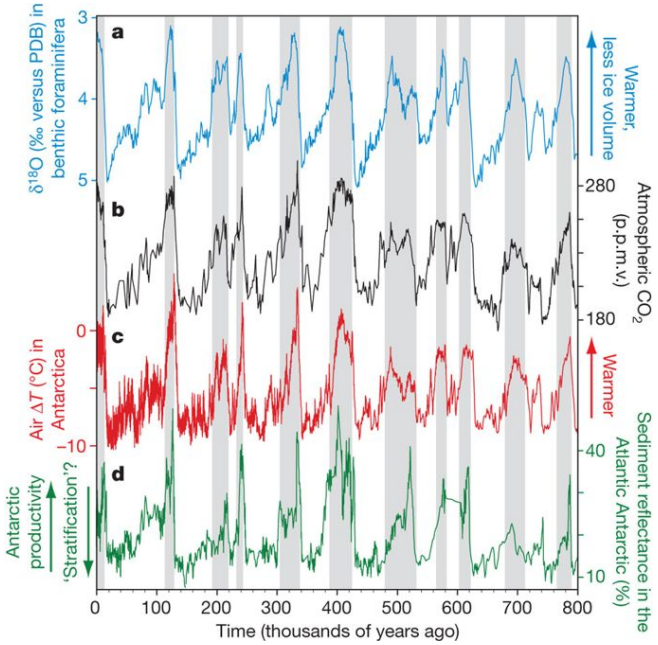

Figure 1: Over the last 800 kyr: a) extent of continental ice caps; b) atmospheric CO_2 concentration; c) air temperature variations; d) oceanic biological productivity. Grey bars show the warm periods, the interglacials. Sigman et al. (2010).

Figure 1 shows the succession of ice ages during the Quaternary (Sigman et al., 2010). They are clearly visible in the Antarctic temperature records (fig. 1C), CO_2 concentration (fig. 1B), and the ice sheets volume (fig. 1A). Although temperature decrease and ice sheet growing can be relatively easily explained with orbital parameters, the tight link between atmospheric CO_2 concentration and temperature is much harder to explain. As it has been shown that CO_2 variations follow temperature variations with a slight delay (Fischer et al., 1999), it is a consequence of the temperature variation rather than a cause.

The mechanisms by which carbon dioxide was removed from the atmosphere are not easily explained. First, the reservoir in which it was stored had to be identified. It quickly became evident that the only reservoir able to react on the millennial timescale and capable of storing that much carbon is the deep ocean (Raven & Falkowski, 1999). The carbon trapped in terrestrial sediments would react far too slowly, and the terrestrial biosphere would not be able to store sufficient carbon. In addition, it is suspected that the terrestrial vegetation released carbon to the atmosphere, as its extent was reduced during ice ages (Jeltsch-Thömmes et al., 2019). As a result, the deep ocean is the only possible reservoir where carbon could have been stored for thousands of years during ice ages. To understand how the deep ocean is capable of storing and releasing carbon, it is important to outline some aspects of the marine carbon cycle, and the mechanisms capable of transferring carbon to the ocean interior.

2.2. Marine carbon cycle

The marine carbon cycle plays a central role in the understanding of the storage of carbon on longer timescales. The main aspects of the marine carbon cycle will be outlined in the following, but it will not be described in details. For a more detailed explanation, the reader is invited to consult Sarmiento & Gruber (2006).

Carbon dioxide is transferred as a function of the difference between the partial pressure of CO_2 (pCO_2) in the atmosphere and in the ocean. The atmospheric pCO_2 at sea level is approximatively constant around the globe, as atmospheric currents mix the troposphere quickly. The atmospheric pCO_2 had values of around 190 ppm during the Last Glacial Maximum (LGM) (Bouttes et al., 2011), and reaches today values of around 410 ppm (Trans & Keeling, 2019). If the oceanic pCO_2 is lower than in the atmosphere, a transfer will occur from the atmosphere to the ocean, in order to equilibrate these concentrations. It is important to note that this transfer can also operate in the other direction, if the oceanic pCO_2 is higher than the atmospheric pCO_2, an outgassing of CO_2 from the ocean will take place. The oceanic pCO_2 is dependent upon multiple

factors. The temperature, salinity, but also the DIC or alkalinity greatly influence the capacity of sea water to dissolve CO_2. The DIC is the dissolved inorganic carbon, which is the total of all carbon species (CO_2, HCO_3^-, CO_3^{2-}) dissolved in the water. The alkalinity is the sum of all the bases dissolved, which determines the capacity of the water to buffer changes in pH. Temperature and salinity act directly on the capacity to dissolve CO2 in the water. DIC and ALK act on the capacity of CO2 to transform into carbonate (HCO_3^-) and bicarbonate (CO_3^{2-}). The more CO_2 is transformed, the lower the pCO_2 would be. The capacity of sea water to hold a great quantity of CO2 is maximized when it is cold and fresh, the DIC is low, and the alkalinity is high (Sarmiento & Gruber, 2006).

2.3. Carbon pumps

The main pathways by which carbon is transferred to the deep ocean are relatively well-known. The first, hinted at in the previous section, is called the gas-exchange pump. When surface waters downwell, they carry along all of the carbon dissolved in the water to the ocean

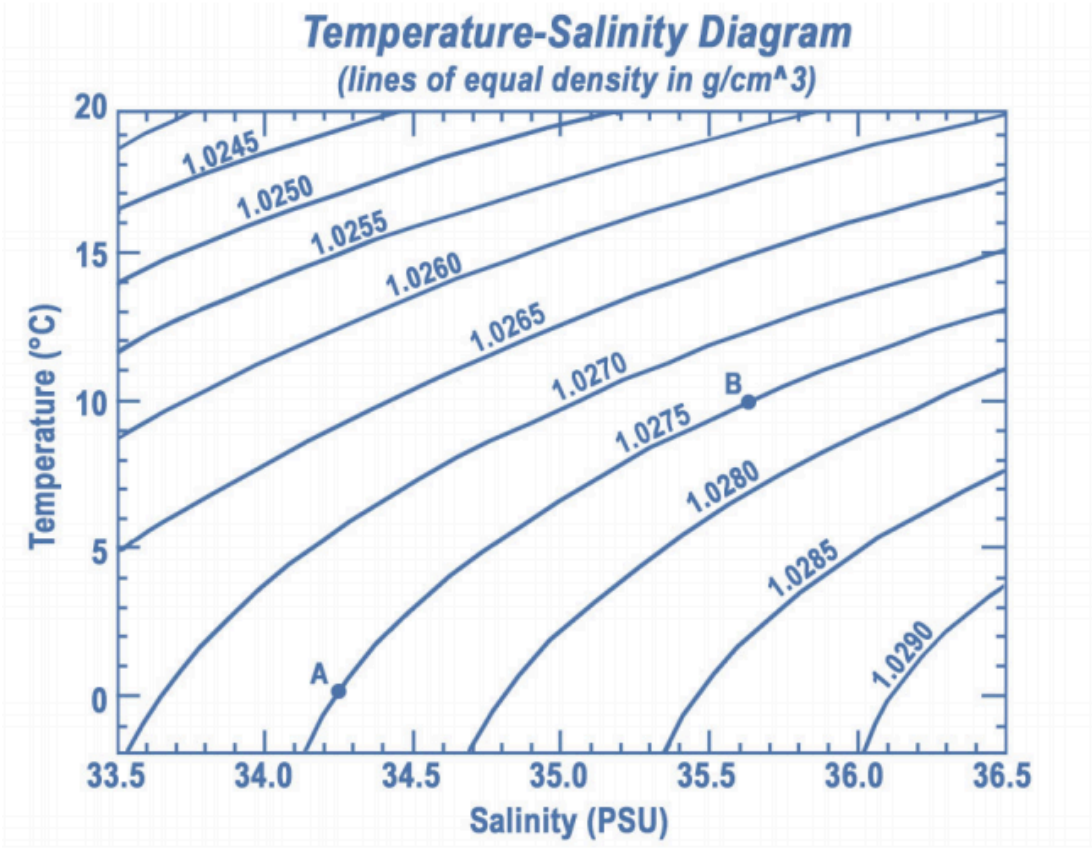

Figure 2: Density of seawater as a function of temperature and salinity. Feldman (2017).

interior. It is here important to remind that the downwelling is conditioned by an increase in density of surface water sufficient to make it dive to the depth. The density of seawater is influenced both by temperature and salinity (fig. 2). The range of variation of temperature and its control on density is greater than that of salinity, until reaching low temperatures, at which point salinity becomes more influent (Feldman, 2017). Consequently, when surface water masses travel to higher latitudes, they progressively get colder, and denser. As seen in the previous section, colder water is also able to dissolve more CO_2. Thus, downwelling water holds a comparatively high quantity of dissolved CO_2.

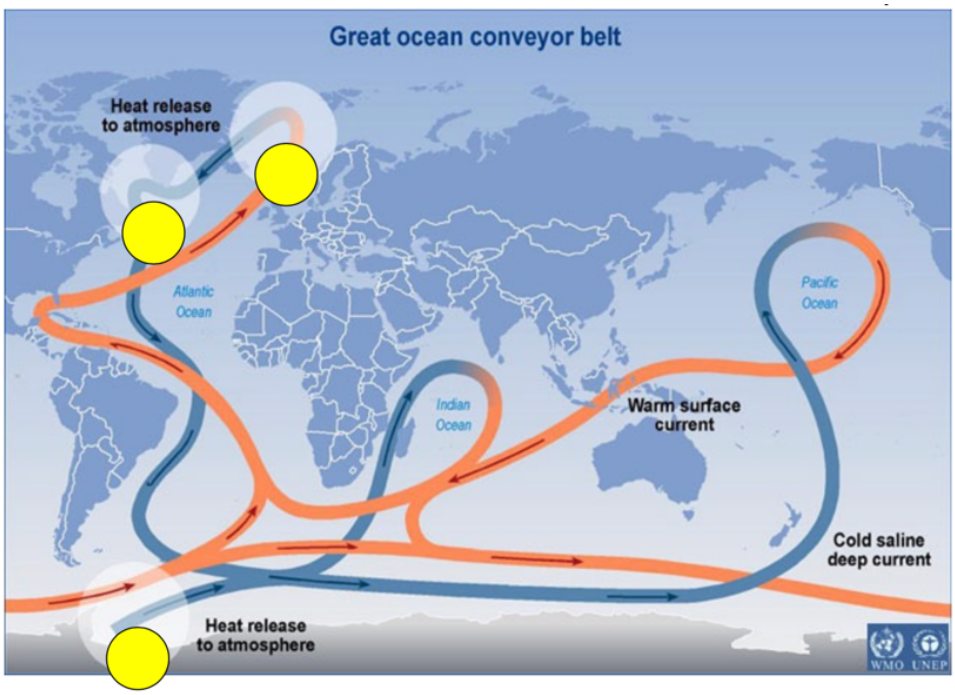

Figure 3: Very simplistic representation of the thermohaline circulation. Gruber (2018).

The main areas where this process occurs is in the North Atlantic and the Southern Ocean (SO). The next figure (fig. 3) illustrates a very schematic representation of the global thermohaline oceanic circulation. It shows that, once at depth, the subsurface water will circulate around the globe before upwelling (Gruber, 2018). This journey will take hundreds, or even thousands of years. Upwelling of deep water is observed in multiple areas of the globe, notably at the equator, but most of the deep water reaches the surface in the SO. Once upwelled, the water will be warmed, and reduce its capacity to hold CO_2, resulting in an outgassing.

In addition to the natural dissolution of CO_2 in the water and its transport to depth, the concentration of dissolved carbon in the deep ocean is continuously increased all along the path of deep water around the globe. This is related to the soft-tissue and carbonate pumps. Depending

on the nutrient availability, and subject to Liebig's law of the minimum, algae will grow in the surface layers of the ocean. They will incorporate dissolved carbon via photosynthesis, which will be replenished by transfer from the atmosphere. At the same time, they will progressively deplete dissolved nutrients necessary for their growth. Once their lifecycle over, they will slowly sink. Most of these particle, called Particulate Organic Carbon (POC), will be reabsorbed by other organisms. A small fraction of the POC produced in the sunlit surface ocean will eventually settle to the ocean floor. The majority of this organic matter will then be remineralized, and transformed into DIC. This process is called soft-tissue pump, and is responsible for the biggest fraction of the total carbon transported to the ocean interior (Sarmiento & Gruber, 2006).

A second process capable to transfer carbon to depth in great quantity is related to the carbonate pump. Some organisms, such as foraminifera, produce carbonate shells, consuming the dissolved carbonate ions in the water. These shells will also sink to depth, and they are collectively called Particulate Inorganic Carbon (PIC). Once settled on the seafloor, the PIC might dissolve and be turned into DIC as well. A small proportion of the total POC and PIC will accumulate in the sediment, where it will be buried for a longer time.

The combined result of these different carbon pumps is a substantial transfer of carbon to the deep ocean. The freshly downwelled water has already a high dissolved CO_2 concentration, owing to its low temperature. As it travels around the globe, its DIC concentration is progressively increased, due to the settling and remineralization of POC and PIC. By the time the deep water ascends to the surface, its carbon concentration is so high that it quickly outgasses to equilibrate with the atmospheric concentration. Consequently, on a millennial timescale, assuming the global oceanic circulation remains unchanged, the net effect of the carbon pumps is close to neutral. An approximatively equal quantity of carbon is transferred to depth than is released to the atmosphere in upwelling zones.

It is also important to note that, when the biological productivity consumes carbon in the surface ocean, phytoplankton also consumes every other nutrients dissolved in the water needed for its growth. It has been shown that all of the main nutrients necessary for phytoplankton growth (N, P and C) are consumed in approximatively constant ratio throughout the ocean, which is known as the Redfield Ratios (Anderson & Sarmiento, 1994). In addition to these main nutrients, biological productivity consumes an array of micronutrients (e.g. Fe, Cu, Mn,...). These elements are needed in lesser quantity, but are necessary nonetheless (Morel & Price, 2003). These macro and micro nutrients are replenished in great quantities in upwelling zone. In these zones, the biological productivity is very strong; despite its strength, the phytoplankton community is not able to consume all of the upwelled nutrients and carbon. In other parts, where the nutrient

concentration is much lower, biological productivity is limited. In these areas, all of the nutrients that are brought are immediately used. The biological productivity is therefore much more efficient there than in upwelling zones.

2.4. Carbon storage

In the previous section, we saw that carbon is naturally brought to the deep ocean in great quantity, but that it is largely compensated by outgassing. To be able to store carbon on longer timescales, outgassing in upwelling areas must be reduced, or the biological pump must become more efficient. As mentioned earlier, the region where most deep water reaches the surface and exchange gases with the atmosphere is the SO. It is therefore probable that the mechanisms contributing to reduce CO_2 outgassing during past ice ages took place in the SO. In addition, atmospheric CO_2 concentration follow the Antarctic temperature records more closely than Greenland's records (Blunier & Brook, 2001; Broecker & Henderson, 1998). This points to a regulator of the CO_2 concentration close to Antarctica.

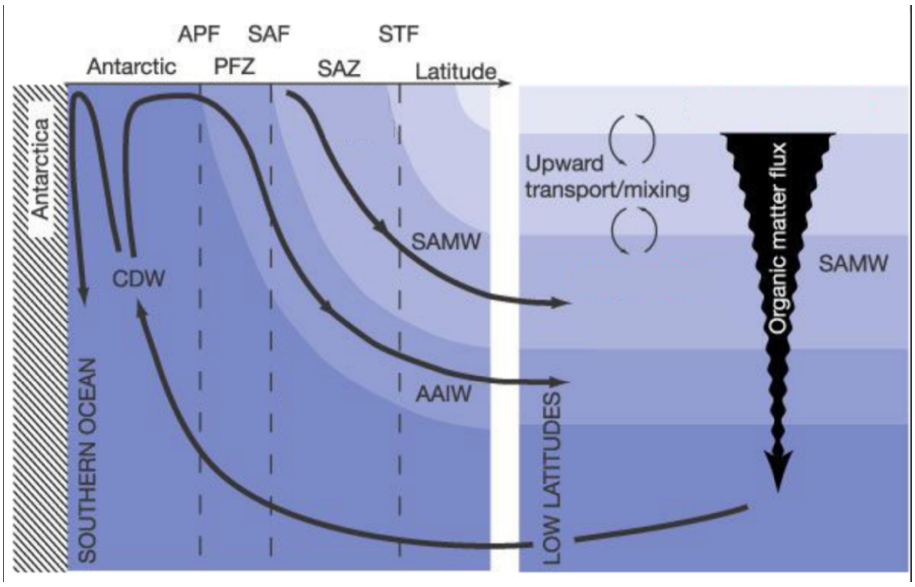

Figure 4: Schematic representation of the water masses circulation in the Southern Ocean. Modified from Sarmiento et al. (2004)

Figure 4 shows a schematic representation of the current situation in the SO. The wind circulation around Antarctica generates Ekman transport of water northwards, which induces upwelling. Circumpolar Deep Waters (CDW) are brought to the surface, in the Antarctic Zone (AZ), bringing a high concentration of nutrients and carbon from below. Despite its high nutrient concentration, surface waters in the AZ have comparatively low primary production. It is one of the few high-nutrient low-chlorophyll (HNLC) zone of the global ocean, where primary production is limited despite high macronutrient concentration (Pitchford & Brindley, 1999).

Nitrate, which is the main limiting nutrient in the global ocean, outside of upwelling zones (Bristow et al., 2017; Moore et al., 2013), is present in the AZ in high concentration. It has been shown that iron is scarce in the AZ, as it is mostly brought to surface waters by upwelling (Frank et al., 2000). This points to iron being the limiting nutrient in this area (Pitchford & Brindley, 1999). As a result, biological productivity is inefficient in the AZ, leaving high concentration of nutrients unconsumed.

As water travels northwards, the upwelled CDW reaches the Polar Front Zone (PFZ), where it meets with subantarctic water, coming from the Subantarctic Zone (SAZ). The subantarctic water has a much lower nutrient concentration than CDW, as it is not replenished by freshly upwelled deep water. As a result, the biological pump is more efficient in the SAZ, consuming a large fraction of the nutrients that are supplied. Consequently, the mixing of the AZ and SAZ water masses in the PFZ creates a zone of very high production (Laubscher et al., 1993). The water masses generated in this area, Antarctic Intermediate Water (AAIW) and Subantarctic Mode Water (SAMW), although partially depleted in nutrients by intense biological activity in the PFZ, have still a relatively high nutrient concentration that will in turn fuel biological productivity in upwelling zones around the world (Sarmiento et al., 2004).

Export production patterns in the AZ are characterized by low biological productivity, limited by iron, and increases strongly while reaching the PFZ. There, high availability of Si is quickly consumed and depleted by the highly competitive diatoms (Egge & Aksnes, 1992). Consequently, diatoms are not found in sediment north of the PFZ, as Si is completely depleted. During the LGM, as the climate was much colder, biological productivity in the AZ was reduced (Jaccard et al., 2013). It has been hypothesized that, with a colder climate during the last ice age, the Southern Ocean might have been more stratified, reducing upwelling (Sigman et al., 2004). Increased stratification could have been caused by a strong increase in salinity of deep water (Francois et al., 1997). Increased stratification, therefore reduced upwelling, diminished the amount of nutrients, and especially iron, brought to the surface. Consequently, biological productivity in the AZ was reduced, and the outgassing of carbon was stemmed. In addition, the upwelling zone in the AZ might have shifted northwards (Toggweiler et al., 2006). As a result, the nutrient-rich deep water would then have been upwelled in the SAZ, where increased availability of iron supplied via the westerlies during the last ice age has been hypothesized (Martinez-Garcia et al., 2014).

In the SAZ, export production is relatively low in the current situation. As stated earlier, the nutrient concentration is much lower than in the AZ, and the biological pump is very efficient. During the colder periods of the last ice age, as the upwelling zone shifted northwards, these

areas became much more productive (Martinez-Garcia et al., 2009). Additionally, increased iron input from eolian dust enhanced the biological productivity in this area (Kumar et al., 1995). To summarize, when the climate became colder, upwelling was reduced in the AZ, which reduced the outgassing of carbon from the deep ocean. Additionally, biological productivity increased in the SAZ. Taken together, these two modes of productivity consistently contributed to enhance carbon storage in the ocean interior during past ice ages, thereby reducing atmospheric CO2 concentrations (Jaccard et al., 2013).

2.5. Eolian dust

Although upwelling of deep water is the main source of nutrients to marine life, it is not the only one. In coastal waters, marine productivity is sustained by nutrient input from land. Similarly, airborne dust can enhance marine life, otherwise Fe-limited, far into sea. Other nutrient sources include, for example, ice-rafted debris.

As stated in the previous section, the main limiting micronutrient for phytoplankton in the Southern Ocean is iron (Boyd et al., 2000; de Baar et al., 1995). Terrestrial eolian sediment provide a source of iron, and fuel algae blooms where plumes of dust reach the ocean surface (Blain et al., 2007). The input of dust is relatively low nowadays, but the combination of a drier and colder climate during the last ice age and more intense glacial erosion greatly increased the generation and transport of dust (Mahowald et al., 1999). Consequently, the amount of lithogenic iron brought by winds during ice ages increased drastically in the SAZ (Kumar et al., 1995; Martinez-Garcia et al., 2014). This greatly enhanced biological productivity, and model outputs show that the combined effect of enhanced water column stratification and iron fertilization in the SO were sufficient to explain the observed CO_2 drawdown during the ice age (Hain et al., 2010; Jaccard et al., 2013; Martinez-Garcia et al., 2014).

The deep ocean has been suggested to have been isolated from the atmosphere during the last ice age, or, at least, its circulation was much slower than observed today (Skinner et al., 2010). As a result, the DIC concentration was substantially higher, due to the continuous remineralization of organic matter and carbonate particles, and the low ventilation of the deep ocean (Sigman et al., 2010). In that context, when the upwelling zone shifted back to its present situation, the ventilation of previously sequestered carbon might have been very rapid, explaining the quick rise of atmospheric CO2 concentration during the last deglaciation (Anderson et al., 2009; Jaccard et al., 2016).

2.6. Aim of this thesis and research questions

As explained in the previous sections, the large-scale variations of atmospheric CO2 during ice age cycles are nowadays relatively well understood. However, the small-scale variations, such as observed during Marine Isotope Stage 3 (MIS 3), illustrated in figure 5, are much harder to explain. The low temporal resolution usually found in marine sediment cores do not allow for an analysis at millennial time scale. Nonetheless, a core retrieved in 2012 by the *RV Marion-Dufresne* is characterized by a very high accumulation rate, all the while covering the entire last glacial cycle. This high accumulation rate will allow a finer analysis of the numerous variations observed during the last ice age. This thesis is part of a project aimed at studying this sediment core. It will be focused on constraining the vertical particle rain rate and assess the feedback transient changes in upwelling may have had on atmospheric CO_2.

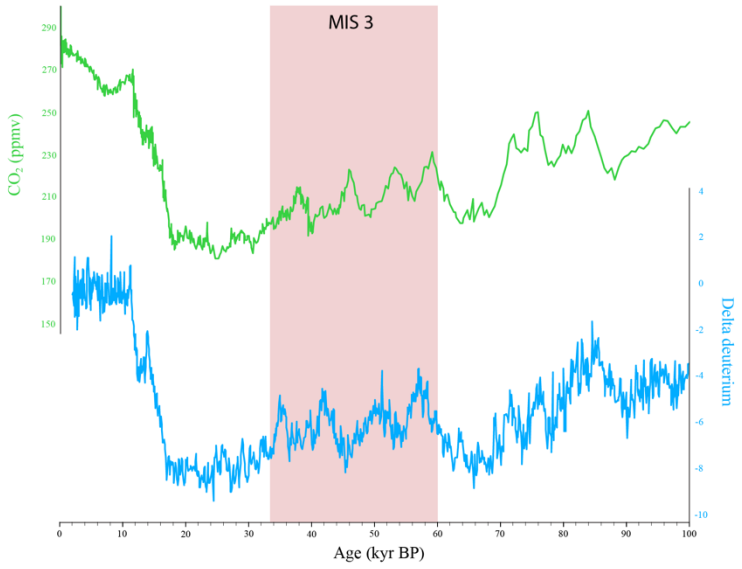

Figure 5: Temperature reconstruction (bottom) and atmospheric CO2 concentration (up) during the last glacial cycle. Marine Isotope Stage 3 is highlighted in the red zone.

The main research questions of this Thesis are:

1) Did eolian dust fertilize biological productivity west of the Kerguelen Plateau ?
2) Did increased biological productivity correlate with atmospheric CO_2 concentration?
3) Did the warm intervals of MIS 3 relate to the same CO_2 release mechanisms as during glacial-interglacial cycles ?
4) Are these mechanisms reversible on millennial time scale ?

3. Methods

3.1. Core location and specifics

Core MD12-3394 was retrieved from the Indian sector of the Southern Ocean (water depth 2310 m, 48°22,54 S; 64°35,17 E). Its location, west of the Kerguelen Islands (fig. 6), is at the edge of the SO. As explained in previous sections, the SO is characterized by a complex system of fronts and water masses. In this Thesis, we are particularly interested by the AZ, the SAZ, and the PFZ that separates them. These zones and fronts are of particular interest, because core MD12-3394 was retrieved in an area situated close to the PFZ (fig. 6). This figure also shows the nitrate concentration in the SO. It is very highly concentrated in the AZ, and decreases sharply in the PFZ; It is almost completely depleted in the SAZ. As a result of its position, this core might have experienced different export production regimes over the last ice age. Assuming the PFZ has been pushed northwards during the cold periods of the ice age (Wefer et al., 2004), the area this core was retrieved in should have passed in an AZ regime. Consequently, the biogenic particle sedimentation rate should be very low during cold periods, and much higher in warmer periods, as the PFZ returned close to that location.

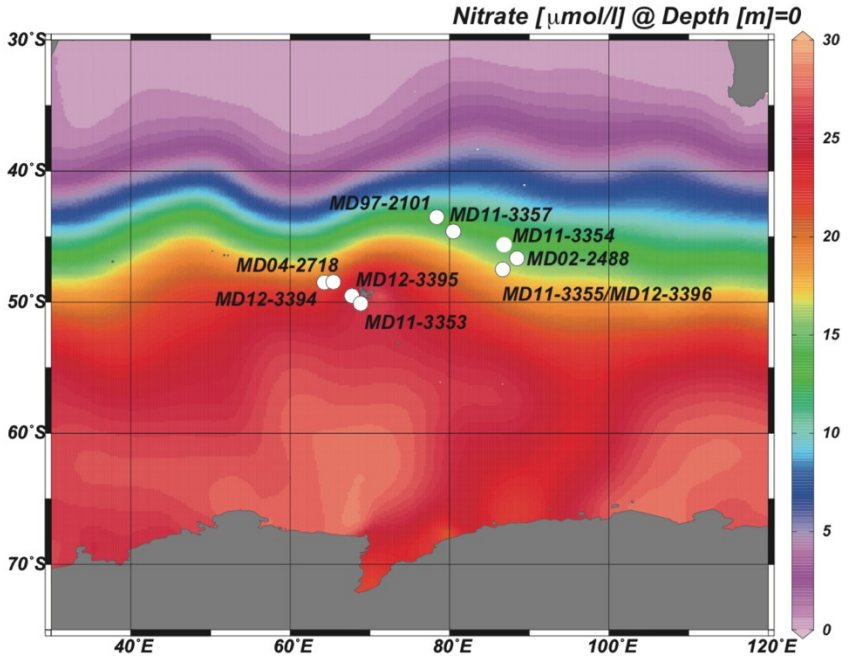

Figure 6: Location of the studied core (MD12-3394) and nitrate concentration of the surface water. The Polar Front is visible where the nitrate concentration drops substantially. The Kerguelen Islands are situated approximatively in the center of the image. (Locarnini et al., 2013)

As discussed earlier, the productivity in the AZ probably decreased substantially during the last ice age (Thöle et al., 2019). Colder climate pushing the PF northwards would therefore not increase productivity, but it would modify the composition of the sediment, in places where the overlying water mass would be changed. Antarctic water masses are rich in nutrients, notably silicate (fig 7). It is an essential nutrient for diatoms, as they produce silica shells called opal. As water travels northwards due to Ekman transport, diatoms progressively deplete dissolved silicate. After reaching the PFZ, it is almost completely depleted. As a result, sediment south of the PFZ would be rich in opal, whereas it would be virtually absent in sediment retrieved north of the PFZ. The main biogenic sediment found there would be calcite, as diatoms do not grow north of the PFZ (Salter et al., 2014). The location of the core studied in this project is in the center of this map (coordinates 48°S; 64°E). There, the silicate concentration, around 15 µmol/kg, is still sufficient for diatoms to grow (Egge & Aksnes, 1992). Consequently, there should be diatoms present in the sediment over the entire glacial cycle. Its proportion might increase during colder period, assuming the PFZ was pushed further north.

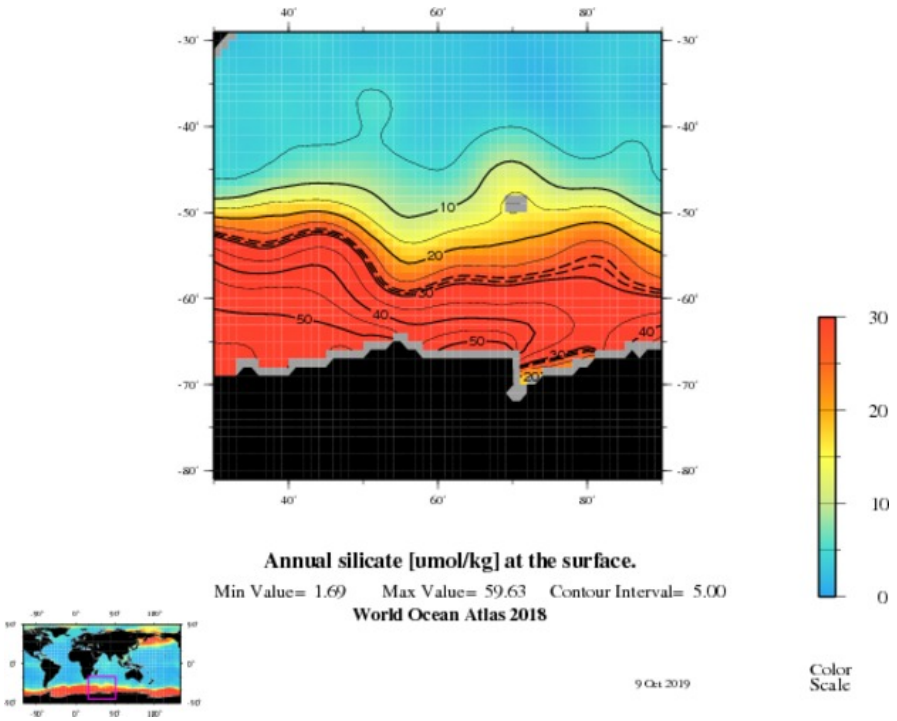

Figure 7: Concentration of dissolved silicate in surface water of the Southern Ocean. This figure shows an area comprised between 30°S and 80°S, and 30°E and 90°E. The coasts of Antarctica are visible at the bottom, and the Kerguelen Islands in the center-right. The MD12-3394 core was taken directly west of the Kerguelen Islands. The silicate concentration at that position is high enough to sustain diatom growth (Egge & Aksnes, 1992). (Locarnini et al., 2013).

3.2. Thorium normalization

The aim of this thesis is to constrain the vertical particle flux in the MD12-3394 sediment core. A general and straight-forward way of estimating sedimentation rate, referred to as Mass Accumulation Rate (MAR), is to date two layers of sediment, and weigh the dry sediment accumulated in between. Although simple, this method relies on very precise dating, which often comes with substantial uncertainties. In addition, it does not take into account redistribution of sediment after deposition. This process, called sediment focusing, erodes some areas and accumulates the eroded sediment elsewhere (fig. 8). This process, hard to predict, may artificially increase the sediment accumulation in some areas. In addition, this is not a constant phenomenon. The sediment focusing can change drastically over a time period.

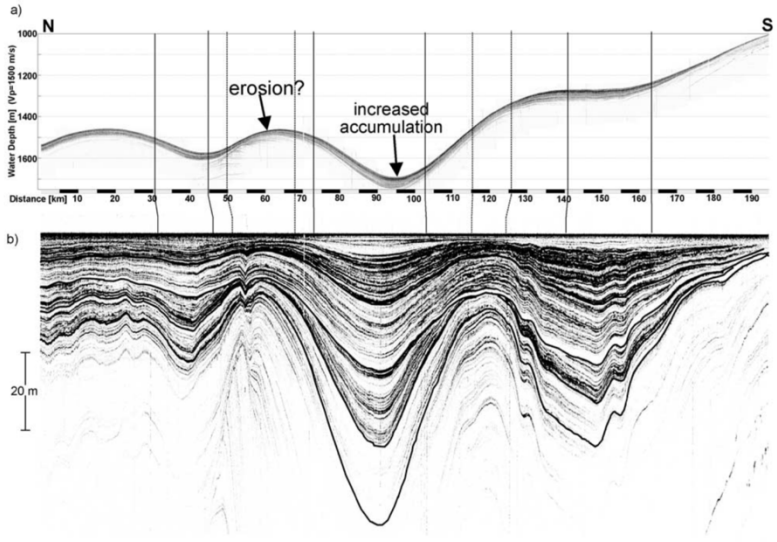

Figure 8: Echo sounder profile of the sea floor along the coast of Namibia. Sediment focusing is visible in depressions. (Francois et al., 2004).

The thorium normalization method has been developed to constrain the vertical particle flux. The main aspects of this method will be described in the following. For a more detailed explanation, the reader is invited to consult Francois et al. (2004).

The radioactive nuclide ^{238}U, which is homogeneously distributed in the global ocean (Chen et al., 1986), produces ^{234}U and ^{230}Th, as well as every other radionuclide of its decay chain, through disintegration. These nuclides are present in seawater in minute quantities due to the weathering of crustal rocks, and subsequent transport through rivers or eolian dust. As ^{234}U is highly soluble in water, its mean residence time in oceans is extremely long, on the order of 320 to 560 kyr (Dunk et al., 2002). ^{234}U is thus well mixed in the oceans, with an approximatively

constant concentration. Therefore, ^{234}U produces ^{230}Th at a uniform and known rate throughout the water column, according to:

$$\beta_{230} = \lambda_{230}^{sw} * A_{U-234}^{sw} = 9.16\,10^{-6}\,year^{-1} * 2910\,dpm\,m^{-3} = 0.0267\,dpm\,m^{-3}yr^{-1} \quad (1)$$

^{230}Th, contrary to its mother nuclide, is highly insoluble. Its mean residence time in seawater is on the order of 20 years (Yu et al., 1996). As soon as ^{230}Th is produced, it is removed from seawater via adsorption on settling particles, and sinks to the seafloor. Models have shown that the production of thorium in the water column is approximatively equal to the flux reaching the seafloor (Henderson et al., 1999). As the ^{234}U concentration in the ocean is well-known and constant, the theoretical ^{230}Th concentration in the sediment can be determined with precision. Comparing this theoretical concentration to the observed concentration in the sediment should yield an estimation of the lateral transport of particles to the sediment core location. In other words, the measured, total ^{230}Th concentration in the sediment comprises the addition of ^{230}Th supplied vertically from the water column, and ^{230}Th transported laterally by bottom currents.

The difficulty resides in the fact that ^{230}Th is not only produced by ^{234}U disintegration in the water column. It is also found in the lattice of eolian dust, or produced by decay of ^{234}U in the sediment. Therefore, thorium has three distinct fractions, referred to as scavenged ^{230}Th for the one produced in the water column, detrital $^{230\text{Th}}$ when brought in the lattice of terrestrial sediment, and authigenic ^{230}Th when produced within the sediment. We are interested here only in scavenged ^{230}Th, as it is the fraction actually brought by the vertical particle flux. Therefore, we need to distinguish the scavenged fraction from detrital and authigenic fractions.

The derivation of the scavenged fraction is described in the following equation:

$$A_{Th-230}^{scav} = A_{Th-230}^{total} - A_{Th-230}^{det} - A_{Th-230}^{auth} \quad (2)$$

The detrital fraction, A_{Th-230}^{det}, is calculated using the ^{232}Th isotope, as it is only present in terrestrial material. By assuming a secular equilibrium between ^{238}U and ^{230}Th, and assuming that the average crustal ratio between ^{238}U and ^{232}Th remains constant through time, the detrital fraction can be approximated via:

$$A_{Th-230}^{det} = A_{U-238}^{det} = A_{Th-232}^{total} * A_{U-238}^{crust}/A_{Th-232}^{crust} \quad (3)$$

The authigenic fraction, A_{Th-230}^{auth}, is calculated via the authigenic ^{238}U. Authigenic uranium can be estimated, as it is directly derived from seawater. As a result, it is equal to the difference of the total measured ^{238}U, minus the detrital ^{238}U, calculated in (3). In the end, we reach the following general formula to calculate the scavenged thorium fraction:

$$A_{Th-230}^{scav} = A_{Th-230}^{total} - \left(A_{U-238}^{det}\right) - \left(1.14 A_{U-238}^{auth}\left(1 - e^{-\left(\frac{0.693t}{75.7}\right)}\right)\right) \quad (4)$$

The scavenged ^{230}Th fraction yields a quantity called Th normalization. When combined with a proxy, it gives an accumulation rate over time of that particular proxy. These proxies can be, for example, the opal concentration in the sediment, or the total organic carbon. Similarly, normalizing the detrital fraction with thorium yields the lithogenic flux.

3.3. Procedure

All of the data of this project were gathered from samples extracted from a single core, MD12- 3394. I collected some of the material, enough so that I could repeat the analyses multiple times, at every depth available. I selected a higher density of samples during MIS 3, the LGM, and the deglaciation. MIS 3 is a period during the last ice age characterized by a rapid succession of cold and warm spells (fig. 5). It took place between around 35 and 60 kyr BP. The LGM is the coldest period of the last ice age, centered around 20 kyr BP. The deglaciation is the period between the LGM and the Holocene, characterized by a rapid increase of both temperature and atmospheric CO2 concentration.

I selected a high density of slices inside those intervals, every 5 to 10 centimeters of depth, and a lower density outside, around every 20 centimeters. I stored the remaining samples for eventual further analysis, and started processing the selected samples.

The first step was to dry the samples. Freeze-drying was considered to be the most adequate procedure to get rid of the water content. After the samples were completely dried, I sub-sampled 0.2 grams of each sample. These sub-samples are the ones that would be processed, and ultimately measured. After weighing them, they were spiked with a solution of precisely known concentration of thorium and uranium isotopes (^{229}Th and ^{236}U). As the concentrations to be measured are extremely low, it is more precise to measure the deviations from a known value rather than to measure an absolute value. For every batch of 8 samples, a standard and a blank were also processed. The standard is a sediment sample of precisely known concentration of each element. The blank only contained the spike.

The next step was to completely digest the samples, meaning that the minerals and organic

compounds constituting the sediment were broken down and dissolved. To dissolve them, they needed to be subjected to a cocktail of nitric, hydrochloric and hydrofluoric acids, and heated up to a temperature of 180°C for 45 minutes. The acids' leftovers were subsequently evaporated. The last step in processing the samples was to separate and purify the samples through an ion exchange resin. This was done to eliminate every ion other than thorium and uranium isotopes. Once the whole procedure was completed, we were left with a set of containers holding the uranium isotopes of each samples, and another set with the thorium isotopes. They were then processed through the Neptune MC-ICP-mass spectrometer to determine the concentrations of uranium and thorium isotopes.

Measuring different isotopes of the same element requires a very fine tuning and high precision measurements. Owing to that, a limited number of samples could be processed and measured. At every batch of measurement, 16 samples were measured, along with 2 standards and 2 blanks. Every batch had to go through two measuring sessions, each lasting 10 hours, in order to measure the uranium isotopes and the thorium isotopes respectively.

3.4. Preliminary analysis

Soon after having been retrieved, the core went through a series of preliminary analysis. As the contact with the atmosphere oxidizes the sediment and modifies their color, the color reflectance measurement has to be generated immediately after their opening. The color reflectance measures the amount of light reflected by the core surface in different bandwidths. The light reflected provides information on the mineral composition of the sediment. Although it does not provide quantitative values for the mineral composition, it is useful to get a first approximation on the general patterns recorded in the core. Bright colors are commonly associated with a high percentage of carbonates. Dark colors can either be a sign of a dominance of opal, lithogenic material, or organic matter.

The X-ray fluorescence (XRF) scanner is used to have a quick approximation of the relative abundance of various elements. It emits X-rays which excite the elements constituting the sediment, which all send back a characteristic wave. The scanner then counts the number of signals of each element that are sent back. This method does not give absolute values for the abundance of each element, but gives relative abundances, with a very high resolution. To have absolute values of the abundance of each element, discrete measurements must be taken on the core, and fitted to a linear regression with the results of the XRF scan. This provides with high resolution absolute values for the entire core. In the scope of this thesis, discrete measurement

could not be done due to the time constraint. Nevertheless, it has been shown that the relation between relative abundances and absolute values is often linear (Eagle et al., 2003). Consequently, I calculated the fluxes of different biogenic proxies, normalized with thorium. These biogenic fluxes have to be considered with caution, as they are based on suppositions subject to be disproved with absolute measurements.

3.5. Proxies

The relative elemental composition of the sediment has been determined by Lena Thöle using the in-house iTrax XRF profiling scanner. From the results of the XRF scan, the abundance of calcium, silicon and barium are used as biogenic proxies. Calcium is a major component of carbonates, which are produced by numerous phytoplankton. It should therefore be correlated with the carbonate shells produced in the upper layers of the ocean. Silicon is the main element of opals, produced by diatoms. It should thus be particularly high in the PFZ. Barium is a proxy for export production, as barite is precipitated when organic matter is remineralized in the water column (Eagle et al., 2003). All of these elements also contain a non-negligible lithogenic component, which needs to be accounted for. Normalizing with iron is a useful approach, assuming Fe is exclusively of lithogenic origin. Consequently, the iron-normalized values for Ca, Si and Ba were used as proxies to estimate the biogenic flux in the core. Barite, calcite and opal are all subject to dissolution in the sediment. However, they are all sensitive to different factors. Barite is sensitive to reducing condition of the water (Dymond et al., 1992). Opal is sensitive to the total sedimentation rate (Archer et al., 1993; Sayles et al., 2001), and carbonate preservation is dependent upon its saturation state in the water (Sarmiento & Gruber, 2006). Consequently, if their abundances are in close correspondence, it is reasonable to assume that the preservation only plays a secondary role in controlling their downcore patterns.

The lithogenic flux is a proxy derived from the thorium normalization measurement and calculation. It gives the flux of lithogenic particles accumulating in the sediment, corrected for the lateral input. This proxy gives an indication on the amount of continental material brought either by wind, or by oceanic currents. As discussed in previous sections, this input of terrestrial dust might have had a crucial importance in glacial to interglacial atmospheric CO_2 concentration. Consequently, this proxy will be compared to the biogenic fluxes in the core, as well as temperature proxy and atmospheric CO_2 concentration measured in Antarctic ice cores.

The last proxies used in this Thesis are a temperature reconstruction, and the atmospheric CO_2 concentration over the last glacial cycle. Both come from Antarctica ice cores, the

temperature was reconstructed from the Vostok ice core, and the CO_2 from the EPICA Dome C ice core (Bereiter et al., 2015). The temperature reconstruction was calculated using the deuterium delta value (Jouzel et al., 2007). Comparing these proxies with the lithogenic flux and the biogenic fluxes will give a better understanding on the mechanisms responsible for the relatively fast variability of CO_2 concentration during the last ice age, particularly during MIS 3.

4. Results

In this section, the results of the thorium normalization will be shown, as well as the different proxies discussed in the previous section. The analysis and discussion of the data will be outlined in the following section.

4.1. Color reflectance

The first step in the analysis of the core was to select which depth intervals were the most promising. As the aim of this Thesis is to study the last ice age, an estimation of the depth it covers was necessary. Unfortunately, an age reconstruction of this core had yet to be done at the time of the samples selection. I consequently had to use other means to roughly match the beginning of the ice age with a depth. I used the color reflectance, which was measured immediately after the core was retrieved.

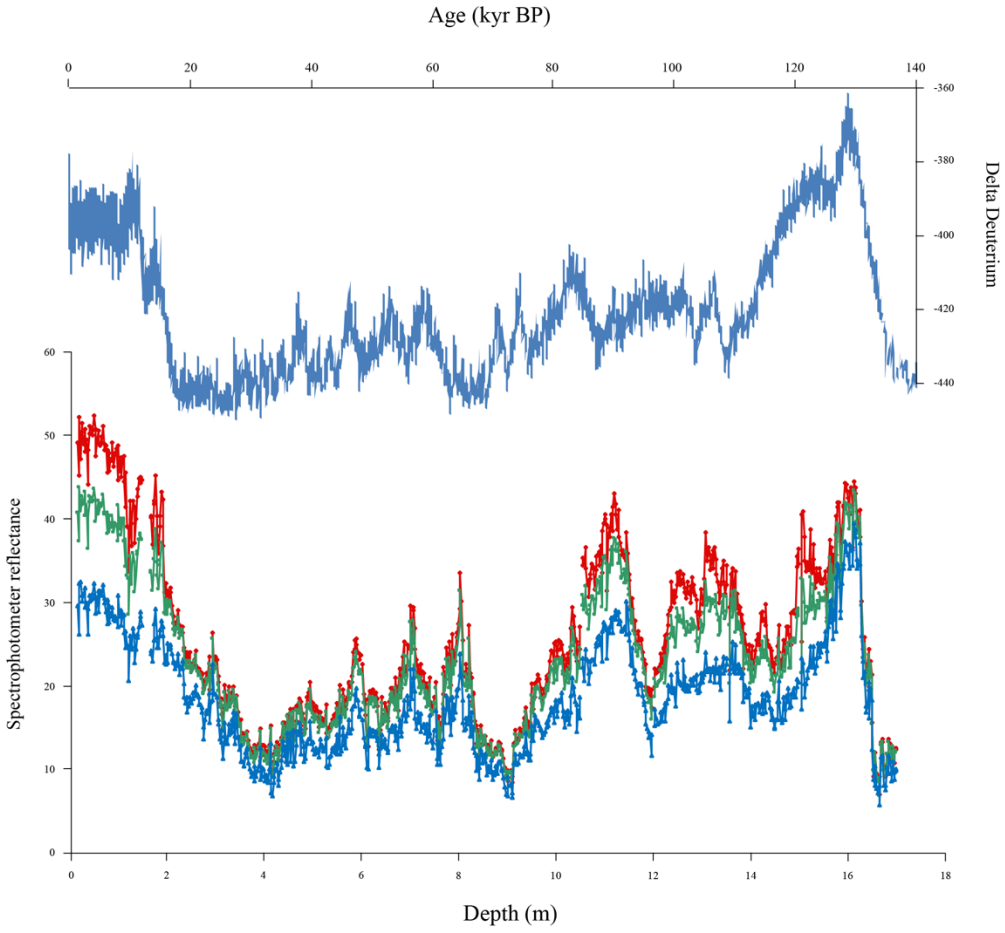

Figure 9: Temperature reconstruction from EPICA Dome C ice core (Bereiter et al., 2015) and color reflectance in MD12-3394. The brighter the sediment is, the higher the reflectance value. The warm interstadials of MIS 3 are easily noticeable between 5 and 8 meters. The LGM is visible at 4 meters.

As we can see on figure 9, there seems to be some correlation between the color reflectance of the studied core and a temperature reconstruction from an Antarctic ice core. It is reasonable to assume that the last ice age is entirely represented. It is visible on the temperature reconstruction approximatively between 20,000 years BP and 130,000 years BP. I estimated that the LGM was at around 4 meters deep in the sediment core, MIS 3 between 5 and 8 meters, and the previous interglacial at around 16 meters deep. The similarities between these two graphs show that this sediment core can be used to reconstruct the vertical particle export during the entire last glacial cycle. Furthermore, the high accumulation rate allows for a very precise analysis.

4.2. Age model

The age model was determined by Xuyuan Ai, at the Max-Plank Institute for Chemistry, University of Mainz. 25 different depths were dated (tab. 1). The first seven tiepoints, between 0 and 2.4 meters, were dated using radiocarbon. The rest of the age model was determined by graphically aligning the TEX86-derived sea surface temperature with the Antarctic temperature records, assuming both properties are in phase. This age model confirmed what was anticipated based on the color reflectance, the sedimentary sequence covers the last glacial cycle, and the

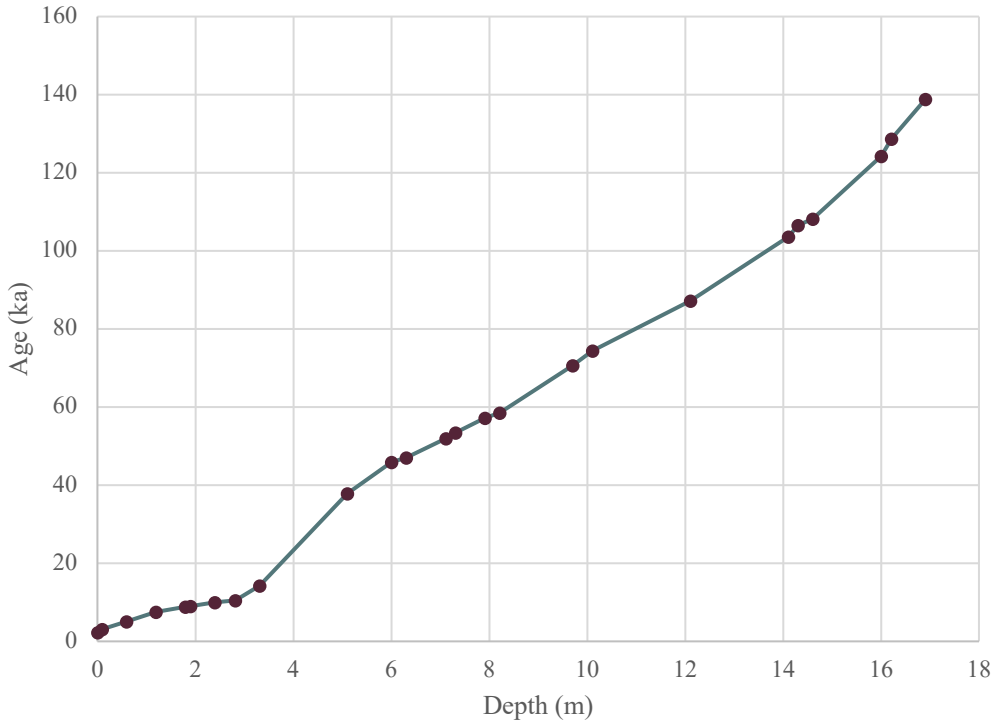

Figure 10 : Dated tiepoints, and age versus depth curve. The relation is fairly linear.

previous interglacial is located at around 16 meters depth. This age model was used in the calculation of the thorium normalization. The intervals between every absolute date were derived using a linear interpolation. As seen in figure 10, the accumulation looks fairly linear during the Holocene. The accumulation regime seems to change around the LGM, but looks again linear afterwards. A linear interpolation in between every tiepoint would therefore be a reasonable approximation.

Table 1: dated depths. Between 0 and 2.4 meters, they were dated using C14. The rest was aligned between SST reconstructions and Antarctic temperature records.

Depth (m)	Age (ka)	Depth (m)	Age (ka)
0	2.36	**7.31**	53.4
0.1	3.12	**7.91**	57.26
0.6	5.14	**8.21**	58.55
1.2	7.45	**9.71**	70.69
1.8	8.90	**10.11**	74.5
1.9	9.06	**12.11**	87.18
2.4	10.03	**14.11**	103.57
2.81	10.53	**14.31**	106.55
3.31	14.25	**14.61**	108.27
5.11	37.82	**16.01**	124.31
6.01	45.91	**16.21**	128.66
6.31	47.02	**16.91**	138.87
7.11	51.99		

4.3. Lithogenic flux

The next figure (fig. 11) shows the lithogenic flux. It is related to the amount of continental material transported by winds or oceanic current to the core location, and subsequent settling to the ocean floor. Due to its isolation, and its position west of the Kerguelen Island, it is expected that most of the terrestrial material has been supplied to the core location from continental sources far away, such as Africa or South America (Lamy et al., 2014). High values are typically associated with a dry and cool climate, resulting in a more extensive continental surface barren of vegetation and subject to eolian erosion (Andersen et al., 1998). The wind blows dust from the continent over the ocean, where it brings essential nutriments to surface waters, fueling algae

blooms where the surface ocean is depleted in nutrients (Kumar et al., 1995; Thöle et al., 2019). The oldest values available here, dating back from 90 kyr BP, show a relatively low amount of dust influx, around 0.15 g/cm^2/ka. A first spike appears at 85 kyr BP, which could correspond to MIS 5b, but, overall, the values remain low until around 70 kyr BP. At that period, which corresponds with MIS 4, the amount of dust input became progressively higher, reaching a peak at around 65 kyr BP, where the value of the lithogenic flux reaches almost 0.4 g/cm^2/ka. Following this, a succession of periods of extremely high followed by moderate dust accumulation is evident. These continue for 20 kyrs, covering all of MIS 3. During MIS 3, the highest values are recorded, at around 0.45 g/cm^2/ka. At the end of MIS 3, the dust input is at around 0.25 g/cm^2/ka. It then slowly increases towards the LGM, where it reaches the value of 0.4 g/cm^2/ka. Following the LGM, during the deglaciation, lithogenic flux dramatically diminishes, until reaching a value of less than 0.05 g/cm^2/ka at the end of the Holocene. The values during the Holocene are much lower than at any point during the last ice age. The values found in this core are relatively low, even during the highest peaks of MIS 3. A study based on cores situated close-by, south and east of the Kerguelen Islands, found values reaching as high as 1 g/cm^2/ka (Thöle et al., 2019). The Kerguelen Islands might have had a much stronger influence on those cores (fig. 6, cores MD11-3357 and MD11-3353), as the westerlies are much more likely to bring terrestrial material from the Kerguelen Islands than in the MD12-3394 core.

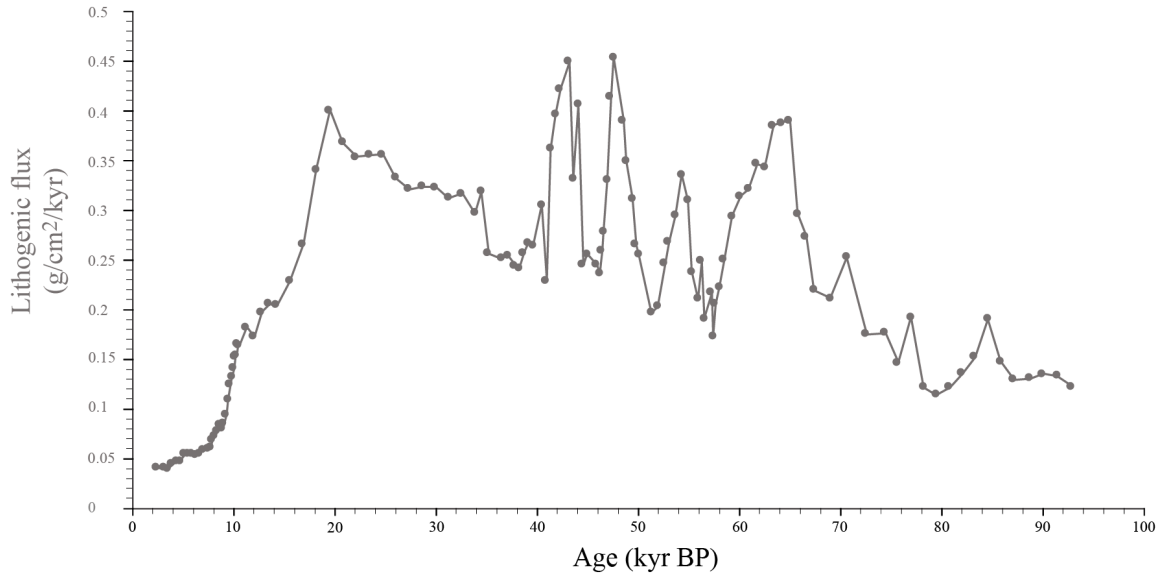

Figure 11: Thorium normalized lithogenic flux.

4.4. XRF scanner

Figure 12 shows the values of the different biogenic proxies used, over the last glacial cycle. These proxies were obtained using the results of the XRF scan. There is a very good accordance in between the different elements, which points to a good preservation of the particles in the sediment. Opals, carbonates and barite are all prone to dissolution once deposited, but they are all sensitive to different conditions, as explained in previous sections. As they all show the same pattern, it is reasonable to assume that the preservation is good in this core. Consequently, they can be used as proxies to estimate the biogenic flux.

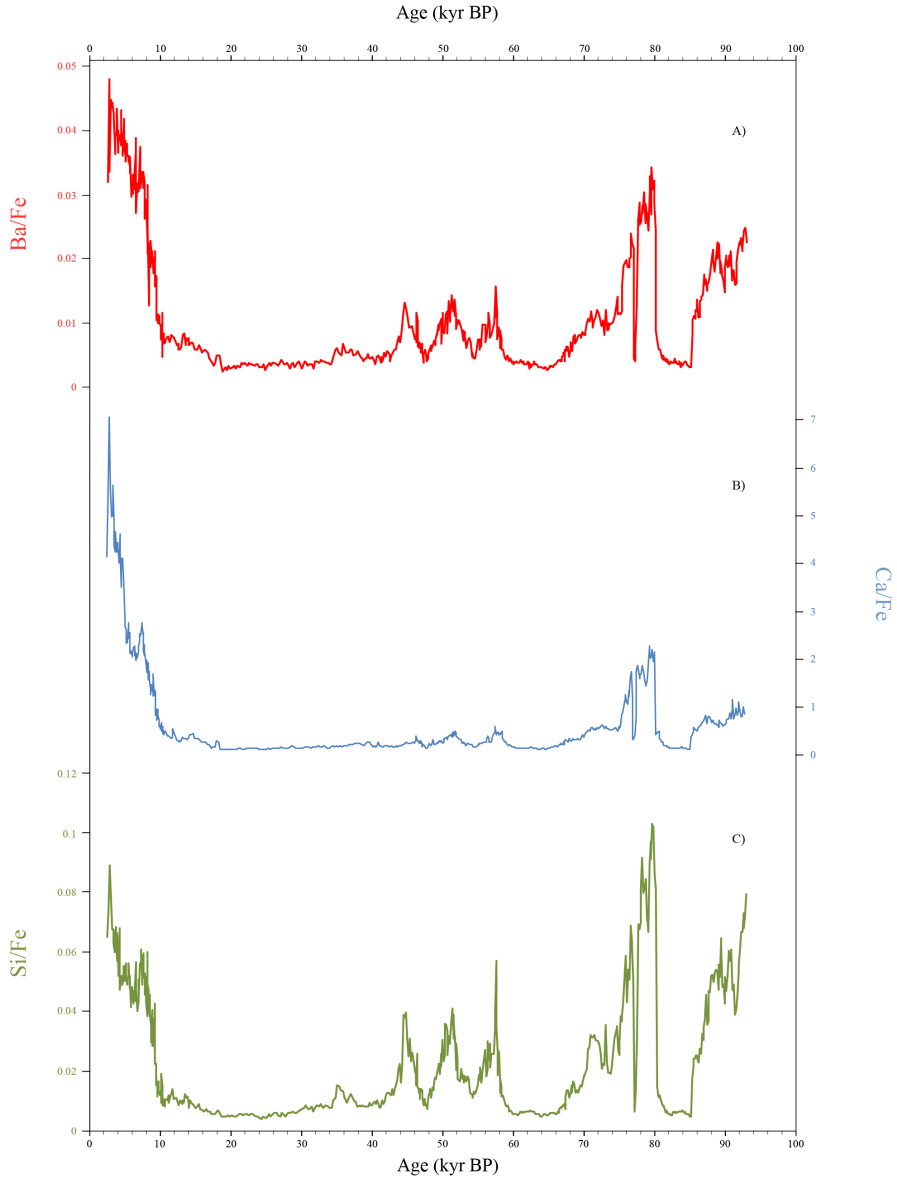

Figure 12: Data extracted from the XRF scan. A) Ba/Fe, proxy for export production. B) Ca/Fe, related to the biogenic carbonate production. C) Si/Fe, opal production proxy.

All of the biogenic proxies show low values when the climate is cold, and higher values in proportion to the warming of the climate. The four different warming peaks of MIS 3 are clearly visible between 35 and 60 kyr BP in the Ba/Fe and the Si/Fe curve, but are much less pronounced in the Ca/Fe curve. The cold periods are characterized with values barely above 0, especially in the Ca/Fe record.

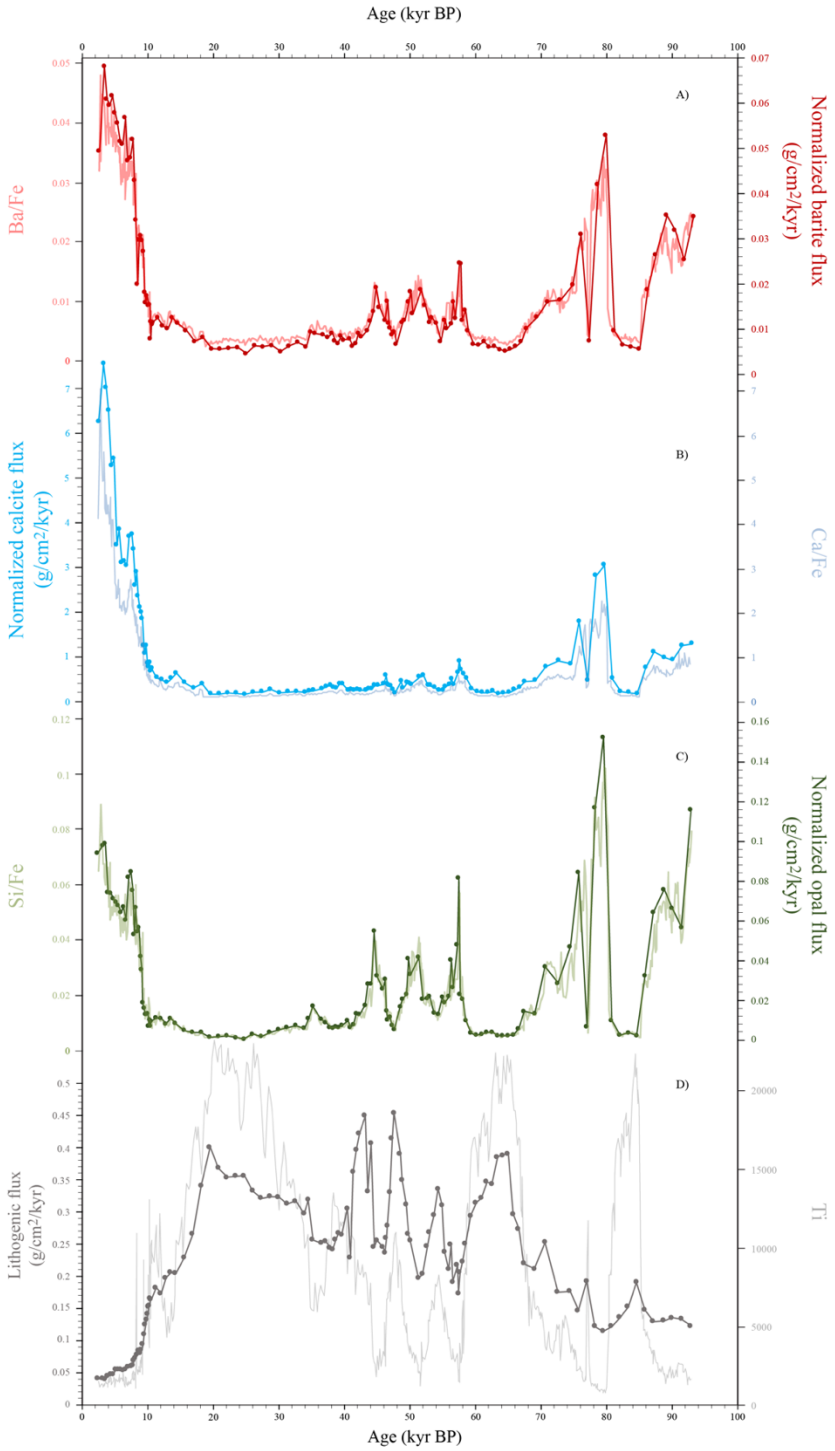

Figure 13: A) Normalized barite flux and XRF scan Ba/Fe. B) Normalized calcite flux and Ca/Fe. C) Normalized opal flux and Si/Fe. D) Lithogenic flux, and Ti counts from the XRF scan.

As stated earlier, the biogenic proxies were normalized with thorium, in order to get actual fluxes, keeping in mind that it is subject to changes after discrete measurement can be performed. Thus, figure 13 shows the Si, Ca and Ba fluxes, normalized with thorium, as well as the lithogenic flux for comparison. The Ti values extracted from the XRF scan are shown to compare with the lithogenic flux. Ti, as Fe, is not found in the biogenic fraction of the sediment, and thus is used to quantify the lithogenic fraction. The three biogenic fluxes are in good accordance, with, overall, low values during colder periods, and higher values during warm periods. The values derived from the XRF data are also plotted as comparison, and the biogenic fluxes normalized with thorium show an excellent correspondence with the XRF data. This suggests that sediment focusing does not play a major role in the sedimentation patterns.

During the ice age, the carbonate flux was extremely low. The only values slightly above 0 $g/cm^2/ka$ are found during the warm peaks of MIS 3, and during MIS 5. During the deglaciation, the amount of carbonate preserved in the sediment increased greatly, reaching more than 7 $g/cm^2/ka$. It is interesting to note that this increase did not happen directly after the LGM, but around 10 kyr BP. The carbonate flux does not seem to be very reactive with a warming climate, as the warmer periods during the last ice age only slightly increased the carbonate flux value. Only with major episode of warming can we see a substantial increase. This might also be due to the threshold pattern carbonate preservation can follow. The opal flux follows the same trend, but seems more reactive to a warming climate. The warm periods during MIS 3 show an increased productivity, reaching almost the level seen during the Holocene. During cold periods, it drops down to almost 0 $g/cm^2/ka$. This low value might be an artifact of the XRF scan and subsequent Fe normalization, as the Fe count is much higher than the Si count. The export production proxy is very similar to the other two. It is also very low during cold periods, and higher when the climate gets warmer. During the deglaciation, it increased substantially higher than during the warm phases of MIS 3. It does not react as much as the opal flux during the warming of MIS 3, but noticeably more than the carbonate flux.

The Ti values are in good correspondence with the lithogenic flux, although they seem to vary much more with climate variations. When the climate is warm, the Ti values are very low, as seen in the warm peaks of MIS 3, or during MIS 5. The cold peaks seem a lot more accentuated, especially during the LGM and MIS 4. The cold peaks of MIS 3 do not record such a strong response in Ti. Overall, the Ti values record the same tendencies as the lithogenic flux in response to a changing climate.

5. Discussion

5.1. Lithogenic flux

The lithogenic flux seems to have a relatively close relationship with Antarctic temperature. When the climate is warm, the dust influx is low, and vice-versa. It is clearly visible during the LGM, which is exactly matched in the temperature record from Antarctica, but also in the atmospheric CO_2 concentration (fig. 14 A, B and D). During the deglaciation, the amount of terrestrial dust is progressively diminished, as the climate became warmer. During warming phases, it is arguable that the lithogenic flux follows the CO_2 curve more closely. The temperature reconstruction from the Vostok ice core shows a rapid warming spanning from around 18 kyr BP to 10 kyr BP, after which it remained relatively stable until the end of the Holocene. In both the dust influx and the CO_2 records, they continued to change well beyond that 10 kyr mark, only stabilizing in the very recent past. The dust load reconstructed from the EPICA Dome C ice core (Lambert et al., 2008; fig. 14 C) shows similarities during the colder periods with the lithogenic flux reconstructed from MD12-3394. During MIS 3, there is no increase of dust concentration in the ice core, whereas it varies substantially in the sediment core. This might be due to the isolation of Antarctica, where significant amounts of dust might only be brought and recorded when the atmospheric dust load is substantial. As a result, during warmer periods, very little dust reached Antarctica.

It is important to note that the eolian dust input at our study site is highly dependent on the source of dust, and the wind pattern. Due to its isolation, dust was brought most likely from Africa (Sicre et al., 2006). Westerlies and ocean currents transport material from the east to the west, therefore the Kerguelen Islands, although close to the core location, might not have much of an impact on the dust input. As stated already, the availability of dust is dependent upon the vegetation cover and the intensity of glacial erosion (Mahowald et al., 1999). As a result, there is a delay between temperature and dust influx, as vegetation needs to recolonize the land after the climate became warmer. This might explain why the warmer stages of MIS 3 do not show a substantial reduction in dust transport compared to the average of the ice age. The vegetation in surrounding areas might not have had time to recolonize the entirety of the land. Another important factor in the lithogenic flux is the wind patterns (Grousset & Biscaye, 2005). The long distance transport of dust from the continents is highly dependent on the dominant winds. A modification of the wind regime, such as a northwards displacement of the westerlies, could artificially substantially increase or diminish the amount of dust brought to the study site,

independently of its availability on continents. This might be an explanation for the very high amount of dust brought during the cold periods of MIS 3, which are even higher than during the LGM.

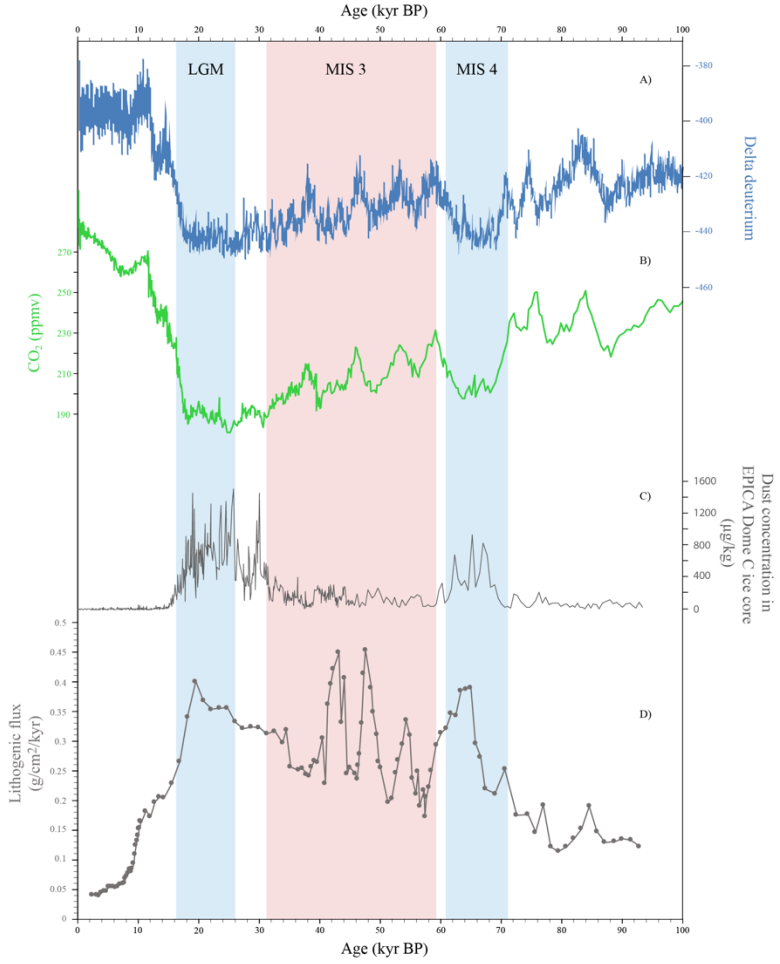

Figure 14: A) Temperature reconstruction from the Vostok ice core (Jouzel et al., 2007). B) Atmospheric CO2 reconstruction from the EPICA Dome C ice core (Bereiter et al., 2015). C) Dust flux from the EPICA Dome C ice core (Lambert et al., 2008). D) Lithogenic flux from MD12-3394

5.2. Biogenic fluxes

Figure 15 shows the biogenic fluxes, the lithogenic flux, and the atmospheric CO_2 concentration. The biogenic fluxes were derived using the Si, Ca, and Ba values of the XRF scan. They were normalized first by Fe, to obtain the biogenic fraction, and then by Th, to remove the fraction supplied laterally. Thus, they show respectively the biogenic opal flux, biogenic carbonate flux, and the total export production. In addition to these fluxes, the original values from the XRF scanner are plotted for comparison.

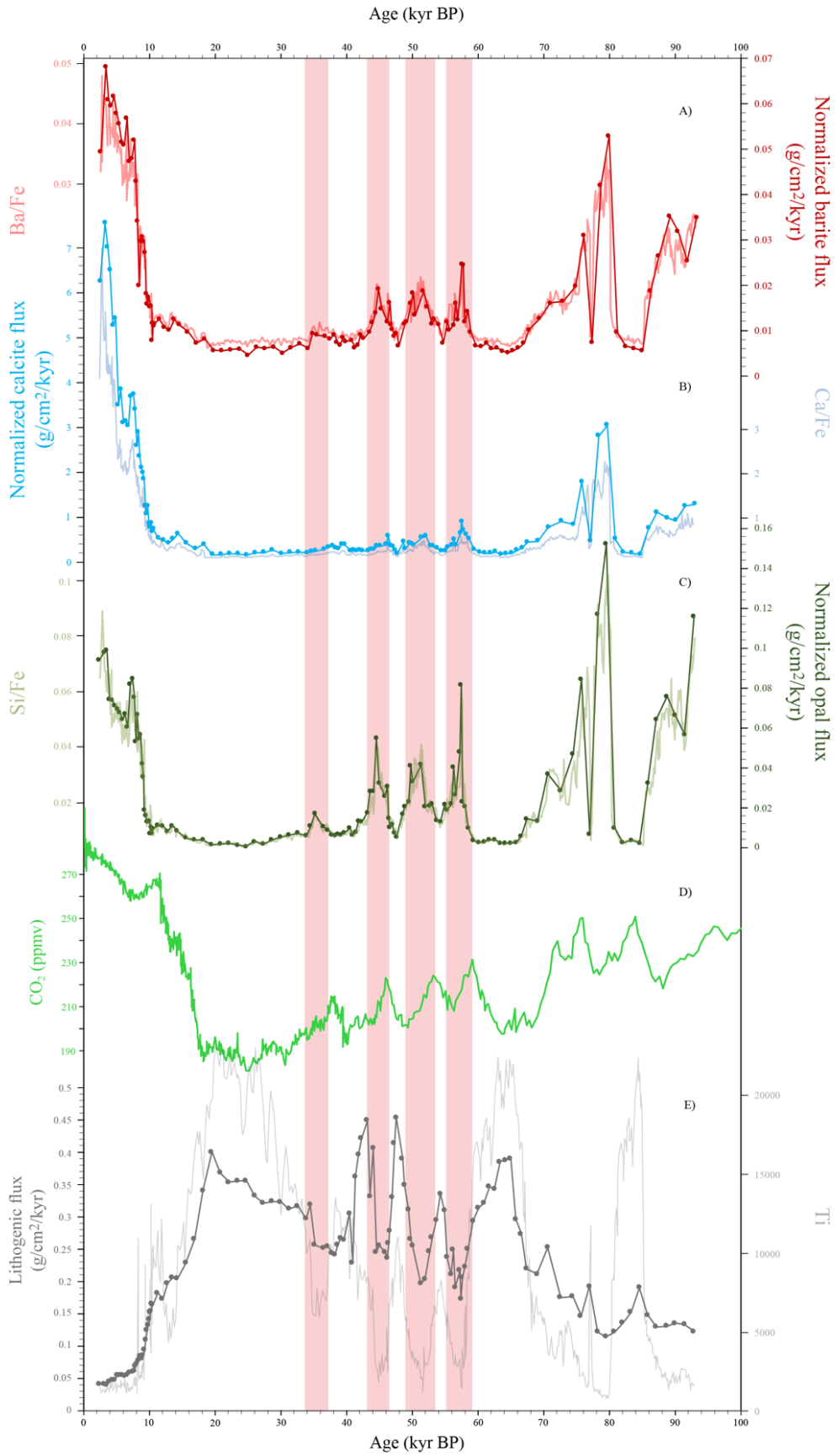

Figure 15: A) Export production and Ba/Fe values. B) Calcite flux and Ca/Fe values. C) Opal flux and Si/Fe values. D) Atmospheric CO2 concentration (Bereiter et al., 2015). E) Lithogenic flux and Ti values from the XRF scan. The red zones represent the warm periods of MIS 3. The lithogenic flux shows an opposite behavior relative to the biogenic fluxes.

Comparing these different values may help to understand which processes are responsible for the CO_2 drawdown, as well as the increased biological productivity. The general understanding of glacial CO_2 drawdown mechanisms, as explained in previous sections, is that the upwelling of deep water became much weaker, bringing far less nutrients and dissolved carbon, to the surface. In that context, the biological pump became more efficient, consuming a large fraction of the nutrients available in the sunlit surface ocean (Studer et al., 2015). A reversal of the upwelling strength to current levels is how the atmospheric CO_2 concentration increased very quickly after the climate became warmer (Jaccard et al., 2016). This would enhance the biological production at the surface, which, eventually, could not keep up with the flow of carbon and nutrient brought to the surface, and CO_2 starts outgassing.

Figure 15 shows that, during the warming periods of MIS 3, the biological productivity was increased in our core. This can be achieved by two distinct mechanisms. Either the upwelling became stronger, as it did during deglaciation, or the terrestrial dust input increased, fertilizing the upper layers of the ocean. This figure clearly shows that during warming periods, at the same time the biological productivity was enhanced, the lithogenic flux became weaker. Consequently, the only option is that the upwelling increased during these periods. This points to similar mechanisms in the CO_2 drawdown and release operating during the large scale cycles, between glacial and interglacial periods, and during small scale cycles, operating at millennial time scale. In addition, it is clear that the biological productivity decreased rapidly when the climate became colder again. This points to a very quick reactivity of the mechanisms influencing the upwelling strength in that area of the Southern Ocean. The very reactive to temperature changes nature of these mechanisms is very clearly recorded in the opal flux (fig. 15 C). During the first and warmest peak of MIS 3, the productivity became almost as high as during the Holocene, and quickly dropped back down to the general ice age situation as the climate became colder, within a few millennia.

A small offset between the atmospheric CO_2 concentration and the biogenic fluxes is apparent in figure 15. This is most likely due to uncertainties in the age model. Assuming the peak in CO_2 and biogenic fluxes are simultaneous, it shows that biological productivity at our core site was not a main contributor to the CO_2 drawdown during the last ice age.

These results, although very promising, need to be taken with caution. As stated earlier, no discrete measurement of the various elements analyzed in the sediment could be done. However, they will be available shortly for subsequent research. Consequently, a linear relation has been assumed between the relative abundances measured by the XRF scanner and the actual

abundance. In addition, the preservation of carbonate, opal and barite in the sediment might be problematic. Even though the good correspondence of their abundance point to a good preservation, it cannot be proven. Last but not least, the age model does come with uncertainties, and the short temporal scale of interest here might be problematic to give definite interpretations. The analysis relies on the peaks observed in CO_2 concentration, biogenic fluxes, and lithogenic flux. The CO_2 concentration was derived from an ice core, more precisely dated, and with a much higher data point density. A few thousand years offset between the CO_2 concentration and the age model derived from this core could modify the interpretations. Nevertheless, the biogenic fluxes and lithogenic flux could not possibly have an offset, and they definitely show that their behavior during MIS 3 is reversed, pointing to an increased upwelling during warmer periods.

6. Conclusion

The primary objective of this Thesis was to constrain the vertical particle flux in core MD12-3394 retrieved from the Southwest Indian Ocean. In that aspect, the results of the normalized particle fluxes conclusively show that this core can be used to analyze the production export during the last ice age with an unprecedented temporal resolution. As the results have shown, the quick and strong increase of export production during the warm phases of MIS 3 point to an acceleration of the upwelling. This brings much needed macro and micro nutrients to the surface, enhancing biological productivity in the Antarctic Zone of the Southern Ocean. Simultaneously, oversaturated carbon is outgassed from the ocean into the atmosphere. This implies that the mechanisms responsible for the rapid increase of atmospheric CO_2 during the deglaciation also operated for a shorter period during the interstadials of the last ice age.

The negative covariation between the lithogenic flux and the biogenic fluxes implies that biological productivity was not fertilized by eolian dust during the last ice age. Furthermore, increased biological activity was always simultaneous with increased temperature and atmospheric CO2 concentration. This further shows that this area of the Antarctic Zone was not influenced by the iron fertilization effect observed in the Subantarctic Zone during the last ice age. The biological productivity strength is mainly dependent upon the upwelling of nutrient rich deep water.

The very quick increase of biological productivity during warming phases, and its rapid decrease as the climate became colder again, show that the underlying processes are fully reversible on a short time scale.

Although the results presented here need to be confirmed, it is clear that a thorough analysis of this core will provide with valuable information to increase our understanding of the small scale variations in atmospheric CO_2 concentration during the last ice age. The thorium normalization data derived in this Thesis will thus be used in numerous subsequent studies based on this sediment core.

Several other proxies could have been calculated, but had to be discarded due to the time constraint. Notably, the opal concentration and the total organic carbon would have given more reliable biogenic proxies. The latter was going to be measured, but, unfortunately, a wrong manipulation during the transport of the samples made it impossible. Further analysis on more reliable biogenic fluxes could provide with stronger evidence for the determination of millennial scale CO_2 variation mechanisms. Analysis of sediment core presenting a similar accumulation rate situated in other parts of the Southern Ocean, notably in the Subantarctic Zone, could give

valuable data to help pinpoint the processes influencing the biological productivity and CO_2 drawdown at a millennial scale during the last ice age.

In addition to increasing our knowledge of past ice ages, the study of atmospheric CO_2 variations regulated by the oceans have utility for studying the future. In our context of manmade rapid atmospheric CO_2 concentration increase, understanding precisely the underlying processes of oceanic carbon uptake are of vital importance. A better grasp of the temporal scale at which these processes operate is crucial for understanding how the deep ocean might accommodate anthropogenic CO_2 emissions.

7. Bibliography

Andersen, K. K., Armengaud, A., & Genthon, C. (1998). Atmospheric dust under glacial and interglacial conditions. *Geophysical Research Letters*, *25*(13), 2281–2284.

Anderson, L. A., & Sarmiento, J. L. (1994). Redfield ratios of remineralization determined by nutrient data analysis. *Global Biogeochemical Cycles*, *8*(1), 65–80.

Anderson, R. F., Ali, S., Bradtmiller, L. I., Nielsen, S. H. H., Fleisher, M. Q., Anderson, B. E., & Burckle, L. H. (2009). Wind-Driven Upwelling in the Souther Ocean and the Deglacial Rise in Atmospheric CO2. *Science*, *323*, 1443–1448.

Annan, J. D., & Hargreaves, J. C. (2013). A new global reconstruction of temperature changes at the Lasrt Glacial Maximum. *Clim. Past*, *9*, 367–376.

Archer, D., Lyle, M., Rodgers, K., & Froelich, P. (1993). What controls opal preservation in tropical deep-sea sediments ? *Paleoceanography and Paleoclimatology*, *8*(1), 7–21.

Bereiter, B., Eggleston, S., Schmitt, J., Nehrbass-Ahles, C., Stocker, T. F., Fischer, H., … Chappellaz, J. (2015). Revision of the EPICA Dome C CO2 record from 800 to 600 kyr before present. *Geophysical Research Letters*.

Berger, A. L. (1992). Astronomical theory of Paleoclimates and the last glacial-interglacial cycle. *Quaternary Science Reviews*, *11*(5), 571–581.

Blain, S., Quéguiner, B., Armand, L., Belviso, S., Bombled, B., Bopp, L., … Wagener, T. (2007). Effect of natural iron fertilization on carbon sequestration in the Southern Ocean. *Nature*, *446*.

Blunier, T., & Brook, E. J. (2001). Timing of millenial-scale climate change in Antarctica and Greenland during the last glacial period. *Science*, *291*(5501), 109–112.

Bouttes, N., Paillard, D., Roche, D. M., Brovkin, V., & Bopp, L. (2011). Last Glacial Maximum CO2 and delta-C13 successfully reconciled. *Geophysical Research Letters*, *38*.

Boyd, P. W., Watson, A. J., Law, C. S., Abraham, E. R., Trull, T., Murdoch, R., … Zeldis, J. (2000). A mesoscale phytoplankton bloom in the polar Southern Ocean stimulated by iron fertilization. *Nature*, *407*.

Bristow, L., Mohr, W., Ahmerkamp, S., & Kuypers, M. M. M. (2017). Nutrients that limit growth in the ocean. *Current Biology Magazine*, *27*, R431–R510.

Broecker, W. S., & Henderson, G. M. (1998). The sequence of events surrounding Termination II and their implications for the cause of glacial-interglacial CO2 changes. *Paleoceanography*, *13*(4), 352–364.

Chen, J. H., Lawrence Edwards, R., & Wasserburg, G. J. (1986). 238-U, 234-U and 232-Th in seawater. *Earth and Planetary Science Letters*, *80*(3–4), 241–251.

de Baar, H. J. W., de Jong, J. T. M., Bakker, D. C. E., Loescher, B. M., Veth, C., Bathmann, U., & Smetacek, V. (1995). Importance of iron for plankton blooms and carbon dioxide drawdown in the Southern Ocean. *Nature*, *373*.

Dymond, J., Suess, E., & Lyle, M. (1992). Barium in deep-sea sediment: A geochemical proxy for paleoproductivity. *Paleoceanography*, *7*(2), 165–181.

Eagle, M., Paytan, A., Arrigo, K. R., van Dijken, G., & Murray, R. W. (2003). A comparison between excess barium and barite as indicators of carbon export. *Paleoceanography*, *18*(1).

Egge, J. K., & Aksnes, D. L. (1992). Silicate as regulating nutrient in phytoplankton competition. *Marine Ecology Progress Series*, *83*, 281–289.

Feldman, G. C. (2017). Density: Seawater Mixing & Sinking. Retrieved October 13, 2019, from Aquarius Sea Surface Salinity from Space website: https://aquarius.oceansciences.org/cgi/ed_act.htm?id=18

Fischer, H., Wahlen, M., Smith, J., Mastroianni, D., & Deck, B. (1999). Ice Core Records of Atmospheric CO2 Around the Last Three Glacial Terminations. *Science*, *283*, 1712–1714.

Francois, R., Altabet, M. A., Yu, E.-F., Sigman, D. M., Bacon, M. P., Frank, M., … Labeyrie, L. D. (1997). Contribution of Southern Ocean surface-water stratification to low atmospheric CO2 concentrations during the last glacial period. *Nature*, *389*, 929–935.

Francois, R., Frank, M., Rutgers van der Loeff, M. M., & Bacon, M. P. (2004). 230Th normalization: An essential tool for interpreting sedimentary fluxes during the late Quaternary. *Paleoceanography*, *19*.

Frank, M., Gersonde, R., Rutgers van der Loeff, M. M., Bohrmann, G., Nürnberg, C. C., Kubik, P. W., … Mangini, A. (2000). Similar glacial and interglacial export bioproductivity in the Atlantic Sector of the Southern Ocean: Multiproxy evidence and implications for glacial atmospheric CO2. *Paleoceanography and Paleoclimatology*, *15*(6), 642–658.

Grousset, F. E., & Biscaye, P. E. (2005). Tracing dust sources and transport patterns using Sr, Nd and Pb isotopes. *Chemical Geology*, *222*, 149–167.

Gruber, N. (2018, February). *General circulation of the Atmosphere and Ocean*. Lecture presented at the ETH Zurich. ETH Zurich.

Hain, M. P., Sigman, D. M., & Haug, G. H. (2010). Carbon dioxide effects of Antarctic stratification, North Atlantic Intermediate Water formation, and subantarctic nutrient drawdown during the last ice age: Diagnosis and synthesis in a geochemical box model. *Global Biogeochemical Cycles*, *24*.

Jaccard, S. L., Galbraith, E. D., Martinez-Garcia, A., & Anderson, R. F. (2016). Covariation of deep Southern Ocean oxygenation and atmospheric CO2 through the last ice age. *Nature*, *530*(210), 207–210.

Jaccard, S. L., Hayes, C. T., Martinez-Garcia, A., Hodell, D. A., Anderson, R. F., Sigman, D. M., & Haug, G. H. (2013). Two modes of change in Southern Ocean Productivity Over the Past Million Years. *Science*, *339*.

Jeltsch-Thömmes, A., Battaglia, G., Cartapanis, O., Jaccard, S. L., & Joos, F. (2019). Low terrestrial carbon storage at the Last Glacial Maximum: Constraints from multi-proxy data. *Clim. Past*, *15*, 849–879. https://doi.org/10.5194/cp-15-849-2019

Jouzel, J., Masson-Delmotte, V., Cattani, O., Dreyfus, G., Falourd, S., Hoffmann, G., … Wolff, E. W. (2007). Orbital and Millenial Antarctic Climate Variability over the Past 800,000 Years. *Science*, *317*(793–796).

Kumar, N., Anderson, R. F., Mortlock, R. A., Froelich, P. N., Kubik, P., Dittrich-Hannen, B., & Suter, M. (1995). Increased biological productivity and export production in the glacial Southern Ocean. *Nature*, *378*.

Lambert, F., Delmonte, B., Petit, J. R., Bigler, M., Kaufmann, P. R., Hutterli, M. A., … Maggi, V. (2008). Dust-climate couplings over the past 800,000 years from the EPICA Dome C ice core. *Nature*, *425*, 616–619.

Lamy, F., Gersonde, R., Winckler, G., Esper, O., Jaeschke, A., Kuhn, G., … Kilian, R. (2014). Increased Dust Deposition in the Pacific Southern Ocean During Glacial Periods. *Science*, *343*(6169), 403–407. https://doi.org/10.1126/science.1245424

Laubscher, R. K., Perissinotto, R., & McQuaid, C. D. (1993). Phytoplankton production and biomass at frontal zones in the Atlantic sector of the Southern Ocean. *Polar Biology*, *13*, 471–481.

Locarnini, R.A., et al., 2013. World Ocean Atlas 2013, Volume 1: Temperature. In: Levitus, S. (Ed.), Mishonov, A. (Technical Ed.), NOAA Atlas NESDIS, vol. 73.

Mahowald, N., Kohfeld, K., Hansson, M., Balkanski, Y., Harrison, S. P., Prentice, I. C., … Rodhe, H. (1999). Dust sources and deposition during the last glacial maximum and current climate: A comparison of model results with paleodata from ice cores and marine sediments. *Journal of Geophysical Research*, *104*(D13), 15895–15916.

Martinez-Garcia, A., Rosell-Melé, A., Geibert, W., Gersonde, R., Masqué, P., Gaspari, V., & Barbante, C. (2009). Links between iron supply, marine productivity, sea surface temperature, and CO2 over the last 1.1 Ma. *Paleoceanography and Paleoclimatology*, *24*.

Martinez-Garcia, A., Sigman, D. M., Haojia, R., Anderson, R. F., Straub, M., Hodell, D. A., … Haug, G. H. (2014). Iron Fertilization of the Subantarctic Ocean During the Last Ice Age. *Science*, *343*, 1347–1350.

Moore, C. M., Mills, M. M., Arrigo, K. R., Berman-Frank, I., Bopp, L., Boyd, P. W., … Ulloa, O. (2013). Processes and patterns of oceanic nutrient limitation. *Nature Geoscience*, *6*, 701–710.

Morel, F. M. M., & Price, N. M. (2003). The Biogeochemical Cycles of Trace Metals in the Oceans. *Science*, *300*, 944–947.

Pitchford, J. W., & Brindley, J. (1999). Iron limitation, grazing pressure and oceanic high nutrient-low chlorophyll (HNLC) regions. *Journal of Plankton Research*, *21*(3), 525–547. https://doi.org/10.1093/plankt/21.3.525

Raven, J. A., & Falkowski, P. G. (1999). Oceanic sinks for atmospheric CO2. *Plant, Cell and Environment*, *22*, 741–755.

Salter, I., Schiebel, R., Ziveri, P., Movellan, A., Lampitt, R., & Wolff, G. A. (2014). Carbonate counter pump stimulated by natural iron fertilization in the Polar Frontal Zone. *Nature Geoscience*, *7*, 885–889.

Sarmiento, J. L., & Gruber, N. (2006). *Ocean Biogeochemical Dynamics*. 41 William Street, Pinceton, New Jersey 08540: Princeton University Press.

Sarmiento, J. L., Gruber, N., Brzezinski, M. A., & Dunne, J. P. (2004). High-latitude controls of thermocline nutrients and low latitude biological productivity. *Nature*, *427*.

Sayles, F. L., Martin, W. R., Chase, Z., & Anderson, R. F. (2001). Benthic remineralization and burial of biogenic SiO2, CaCO3, organic carbon, and detrital material in the Southern Ocean along a transect at 170°W. *Deep-Sea Research II*, *48*, 4323–4383.

Sicre, M.-A., Labeyrie, L., Ezat, U., Mazaud, A., & Turon, J.-L. (2006). A 27 kyr terrestrial biomarker record in the southern Indian Ocean. *Geochemistry, Geophysics, Geosystems*, *7*(7).

Sigman, D. M., Hain, M. P., & Haug, G. H. (2010). The polar ocean and glacial cycles in atmospheric CO2 concentration. *Nature*, *466*, 47–55.

Sigman, D. M., Jaccard, S. L., & Haug, G. H. (2004). Polar ocean stratification in a cold climate. *Nature*, *428*, 59–63.

Skinner, L. C., Fallon, S., Waelbroeck, C., Michel, E., & Barker, S. (2010). Ventilation of the Deep Southern Ocean and Deglacial CO2 rise. *Science*, *328*, 1147–1151.

Studer, A. S., Sigman, D. M., Martinez-Garcia, A., Winckler, G., Kuhn, G., Esper, O., … Haug, G. H. (2015). Antarctic Zone nutrient conditions during the last two glacial cycles. *Paleoceanography and Paleoclimatology*, *30*(7).

Thöle, L. M., Amsler, H. E., Moretti, S., Auderset, A., Gilgannon, J., Lippold, J., … Jaccard, S. L. (2019). Glacial-interglacial dust and export production records from the Southern Indian Ocean. *Earth and Planetary Science Letters*, *525*.

Toggweiler, J. R., Russell, J. L., & Carson, S. R. (2006). Midlatitude westerlies, atmospheric CO2, and climate change during the ice ages. *Paleoceanography and Paleoclimatology*, *21*.

Trans, P., & Keeling, R. (2019). Trends in Atmospheric Carbon Dioxide. Retrieved October 10, 2019, from National Oceanic and Atmospheric Administration website: https://www.esrl.noaa.gov/gmd/ccgg/trends/mlo.html

Wefer, G., Mulitza, S., & Ratmeyer, V. (2004). *The South Atlantic in the Late Quaternary. Reconstruction of Material Budgets and Current Systems*. Berlin: Springer-Verlag.

Yu, E.-F., Francois, R., & Bacon, M. P. (1996). Similar rates of modern and last-glacial thermohaline circulation inferred from radiochemical data. *Nature*, *379*, 689–694.

8. Appendix

Table 2: Age model, lithogenic flux and Th normalization values for all of the measured samples

Depth (cm)	Age (ka)	Lith flux [g/(cm^2*kyr)]	Th normalization [g/cm^2/ka]
1	2.36439338	0.040789646	1.5297502
11	3.12296225	0.040972976	1.46751457
21	3.52644108	0.039782988	1.66155932
31	3.92991992	0.04459087	1.46848087
41	4.33339875	0.046820743	1.4569904
51	4.73687759	0.047751343	1.63284532
61	5.14035642	0.054320392	1.86295735
71	5.5264044	0.054715641	1.73267991
81	5.91245237	0.055396714	1.86114091
91	6.29850035	0.05301097	2.0417614
101	6.68454833	0.054855498	2.76468481
111	7.0705963	0.059157009	2.04489729
121	7.45664428	0.059529754	2.17646209
131	7.69699537	0.060424122	2.00751209
141	7.93734647	0.068683916	2.2284102
151	8.17769756	0.072841897	2.38617837
161	8.41804865	0.077698787	2.96618706
171	8.65839975	0.083019722	2.21350467
181	8.89875084	0.079488651	2.35373961
191	9.06239683	0.084347822	2.12617947
201	9.25639012	0.093816344	2.02212001
211	9.45038342	0.108111985	1.88345407
221	9.64437671	0.123555082	1.86059106
231	9.83837001	0.131076067	1.84873646
241	10.0323633	0.139587189	1.97979923
251	10.1567725	0.151431425	1.63341522
261	10.2811817	0.152123777	1.67380511
271	10.4055908	0.16343721	1.74195034
281	10.53	0.162184376	1.58160956
291	11.274	0.180620839	1.98980127
301	12.018	0.170909149	2.02954165
311	12.762	0.195194128	2.45293658
321	13.506	0.203584588	2.39448333
331	14.25	0.202155837	2.0964397
341	15.5594444	0.22627772	1.52913309
351	16.8688889	0.262993073	1.48919089
361	18.1783333	0.337067175	1.62891044
371	19.4877778	0.396038938	1.66852112
381	20.7972222	0.364021281	1.54071269

391	22.1066667	0.349631969	1.48305647
401	23.4161111	0.351586682	1.30179667
411	24.7255556	0.351915117	1.49160703
421	26.035	0.328821479	1.25925965
431	27.3444444	0.318019038	1.29587529
441	28.6538889	0.320324547	1.29578608
451	29.9633333	0.319447049	1.50999275
461	31.2727778	0.309160859	1.62925517
471	32.5822222	0.313262483	1.7931186
481	33.8916667	0.293738315	1.86359205
486	34.5463889	0.315353467	2.62003738
491	35.2011111	0.253555273	2.33967545
501	36.5105556	0.248606018	2.21025603
506	37.1652778	0.2517158	2.51371128
511	37.82	0.242068454	1.49160857
516	38.2694444	0.238687026	3.21108912
521	38.7188889	0.254594284	3.44539644
526	39.1683333	0.263826911	1.78875234
531	39.6177778	0.261144245	1.48656208
541	40.5166667	0.301775018	3.68250326
546	40.9661111	0.226518893	3.00623852
551	41.4155556	0.357757701	4.85293483
556	41.865	0.392503162	2.65128274
561	42.3144444	0.417495748	2.18235227
571	43.2133333	0.444454129	5.48048027
576	43.6627778	0.328203772	6.2035809
581	44.1122222	0.401697292	2.3029758
586	44.5616667	0.242696828	5.08043052
591	45.0111111	0.252872559	3.85336295
601	45.91	0.242285039	3.81934814
611	46.28	0.233419621	1.96189347
616	46.465	0.256190993	2.3420527
621	46.65	0.275990212	1.92518098
631	47.02	0.327288072	2.04367049
636	47.330625	0.409395547	2.23123632
641	47.64125	0.448902344	2.04607152
656	48.573125	0.385891346	2.54512427
661	48.88375	0.345820373	2.79222429
671	49.505	0.308199881	2.87543224
676	49.815625	0.262797176	4.29695065
681	50.12625	0.252706705	3.69169865
701	51.36875	0.194942101	5.21386291
721	51.99	0.201192277	2.95689485

726	52.695	0.244008388	3.76113249
736	53.0475	0.264962797	3.33032371
746	53.7216667	0.291645604	2.97083966
756	54.365	0.332017596	3.14158014
761	55.0083333	0.306709528	2.76977143
771	55.33	0.235839172	3.28589127
776	55.9733333	0.208858035	3.78960334
781	56.295	0.246363496	7.90848508
791	56.6166667	0.189182983	3.0481432
796	57.26	0.215010088	5.79891255
801	57.475	0.171613478	4.62082024
811	57.69	0.20337329	4.90545732
821	58.12	0.220729173	4.44700142
831	58.55	0.248300276	1.91827055
841	59.3593333	0.291071894	1.66523331
851	60.1686667	0.311137215	1.78702379
861	60.978	0.317972939	1.72855391
871	61.7873333	0.34281777	1.91551159
881	62.5966667	0.339392457	1.75117851
891	63.406	0.381324839	1.8203291
901	64.2153333	0.383528685	1.79839895
911	65.0246667	0.385907065	1.84668316
921	65.834	0.293047811	1.38523548
931	66.6433333	0.270662668	1.3875655
951	67.4526667	0.217181838	2.14720186
971	69.0713333	0.209326764	2.22169923
991	70.69	0.24995424	2.86646323
1011	72.595	0.173344331	2.33110566
1031	74.5	0.17496556	3.31168479
1051	75.768	0.145323163	3.32877029
1071	77.036	0.190221898	3.44126918
1091	78.304	0.120588111	4.47540254
1111	79.572	0.113201686	7.05599787
1131	80.84	0.120881319	4.67375069
1151	82.108	0.134992285	3.27320952
1171	83.376	0.151070366	2.21930031
1191	84.644	0.188623951	1.9352695
1211	85.912	0.146527982	2.27618437
1231	87.18	0.128190615	3.38149067
1251	88.819	0.129574337	4.18782179
1271	90.0596036	0.133819938	4.71352248
1291	91.4994055	0.132259229	3.90662625
1311	92.9392073	0.121701204	5.61572875

9. Acknowledgments

This Thesis could not have been made without the help and support of numerous people. First, I want to particularly thank Prof. Samuel Jaccard for the opportunity to work on that project, his supervision, and his help during the entirety of this Thesis. In addition, I want to thank him for the opportunity to join the CROTALE expedition in the Indian Ocean in Ferburary and March 2019.

I also want to especially thank my advisor Eri Amsler, for having taught me the lab procedure, and her very patient help throughout this project. She also helped me greatly with the analysis of the data. Her expertise in the lab and with the measuring equipment were absolutely vital to this project. Additionally, her upbeat and positive attitude helped me greatly.

I also want to thank Lena Thöle, who did valuable measurements and sample processing prior to my Thesis, as well as for her help in the lab. I am also very grateful to Dr. Martin Wille, who gave precious help with the Neptune mass-spectrometer, and who was always available to fix numerous issues with the equipment. In addition, I want to thank Juljana Krbanjevic, who helped me with several equipment, notably the freeze-drier. My analysis could not have been done without the age model calculated by Xuyuan Ai, at the Max-Plank Institute for Chemistry, University of Mainz, I thus thank her for having done these measurements and sent them in time for the analysis of this Thesis. I am also grateful to the Oeschger Centre for the financial help during this project.

Declaration of consent

on the basis of Article 30 of the RSL Phil.-nat. 18

Name/First Name: Thévenaz Antoine

Registration Number: 12-426-599

Study program:

Bachelor ☐ Master ☑ Dissertation ☐

Title of the thesis: Constraining the vertical particle export during the last glacial cycle in Southern Indian Ocean sediment core

Supervisor: Prof. Samuel Jaccard

I declare herewith that this thesis is my own work and that I have not used any sources other than those stated. I have indicated the adoption of quotations as well as thoughts taken from other authors as such in the thesis. I am aware that the Senate pursuant to Article 36 paragraph 1 litera r of the University Act of 5 September, 1996 is authorized to revoke the title awarded on the basis of this thesis.

For the purposes of evaluation and verification of compliance with the declaration of originality and the regulations governing plagiarism, I hereby grant the University of Bern the right to process my personal data and to perform the acts of use this requires, in particular, to reproduce the written thesis and to store it permanently in a database, and to use said database, or to make said database available, to enable comparison with future theses submitted by others.

Place/Date

Bern, 21. October 2019

Signature A. Thévenaz